The Pennsylvania State University

The Graduate School

Department of Geosciences

MECHANISMS OF SULFUR ISOTOPE FRACTIONATION DURING

THERMOCHEMICAL SULFATE REDUCTION BY AMINO ACIDS: *IMPLICATIONS FOR*

THE MIF-S RECORD IN ARCHEAN ROCKS

A Thesis in

Geosciences

by

Andrew Chorney

Submitted in Partial Fulfillment

of the Requirements

for the Degree of

Master of Science

August 2014

The thesis of Andrew Chorney was reviewed and approved by the following:

Hiroshi Ohmoto
Professor of Geosciences
Thesis Advisor

Matthew Fantle
Assistant Professor of Geochemistry

Christopher House
Professor of Geosciences,

Demian Saffer
Professor of Geosciences
Interim Associate Head of Graduate Programs and Research

*Signatures are on file in the Graduate School

ABSTRACT

The understanding of the evolution of the earth's early atmosphere has largely been based on the behavior of the multiple isotopes of sulfur. However experiments designed to mimic fractionation in both an oxygen poor atmosphere through SO_2 photolysis and a presumably oxygen rich atmosphere though thermochemical sulfate reduction (TSR) have thus far been unable to confirm a mechanism capable of creating the mass independent fractionation of sulfur (MIF-S) signatures observed in Archean age rocks. This has created much controversy in how the MIF-S record is used to determine Archean environments. However large amounts of geochemical evidence suggest at least appreciable amounts of oxygen in the atmosphere and ocean at different stages through the Archean. This has motivated us to further explore TSR as a source of MIF-S through a rigorous investigation of how chemical speciation, experimental conditions, time, and rate effect sulfur isotope fractionation. Our results show the importance of initial sulfur redox state and chemistry, temperature, and organic reductant type in creating characteristic mass dependent and independent fractionations. Including previous TSR results (Watanabe et. al., 2009 and Oduro et. al., 2011) we report increased $\delta^{34}S$ and $\Delta^{36}S$ fractionation in TSR products to 15.50‰ and 1.5‰ respectively and increased $\Delta^{33}S$ range from -.22 to 2.30‰ in H_2S largely through the use of mixtures of glycine and alanine. In sulfate we observe $\delta^{34}S$ fractionation between 0.00 and 7.85‰ and $\Delta^{33}S$ fractionation between -.15‰ and 0.0‰. By quantifying fractionation amongst different sulfur bearing products produced during experiments and collected at experiment conclusions in addition to characterizing the effects due to various experimental conditions we are also able describe a schematic framework for the isotope effects during various steps of TSR. Fractionation from the magnetic isotope effect (MIE), the vibrational energy discontinuity effect (VEDE), first described for heterogeneous reactions by Lasaga et. al, 2008, and normal stable isotope mass dependently driven kinetic isotope effects (KIE) are utilized in this schematic to describe the experimental results. The MIE and VEDE are responsible for the MIF-S signatures observed in organic polysulfides and H_2S at high temperatures.

Additionally the effects of these mechanisms are greatly influenced by amino acid type, specifically in experiments that use a mixture of glycine and alanine. The VEDE and KIE are responsible for δ^{34}S fractionation with the overall effect of producing sulfide depleted in ^{34}S at lower temperatures. The interplay of these mechanisms is responsible for Δ^{33}S and δ^{34}S trends observed in sulfides and sulfate samples. Based on this proposed schematic for sulfur isotope fractionation during TSR major trends and features in the Archean Δ^{33}S vs. δ^{34}S and Δ^{36}S vs. Δ^{33}S record can be interpreted. Our results confirm that MIF-S signatures observed in natural samples are a product of depositional environment and possibly reflect characteristics of reactions specific to sedimentary basin conditions and early earth's tectonic regime.

TABLE OF CONTENTS

LIST OF FIGURES

LIST OF TABLES

ACKNOWLEDGEMENTS

1. Introduction

1.1 Background

The preservation of MIF-S in Archean age rocks has been interpreted by most geochemist as the result of the photochemical reactions in an oxygen poor atmosphere (Farquhar 2000; Pavlov and Kasting 2002). This is because most researchers believe the only mechanism capable of creating the MIF-S signatures and trends in the Archean is the photo-dissociation of SO_2 gas by ultraviolet radiation. Correlation between MIF-S signatures and organic content of sediments in the Archean (Ohmoto et. al., 2006a.) as well as in rocks younger than 2.4 Ga (Bontognali et. al., 2012; Young et. al., 2013) suggest that the isotopic composition of these samples may be influenced by depositional processes. An alternative MIF-S producing mechanism may explain enrichments and isotope fractionations in Cr, Mo, Ce, Re and Fe (Kerrich and Said 2011; Ohmoto et al., 2014; Kendall et. al., 2010; Czaja 2012; Frei at al., 2009) that provides evidence for appreciable levels of oxygen in the Archean atmosphere as well as the surface and deep ocean. Furthermore, while the $\Delta^{33}S$-$\delta^{34}S$ trends in the products of broadband SO_2 photolysis experiments have been able to match those observed in modern stratospheric sulfate aerosols, they have not been able to reconcile those observed in the sedimentary record (Whitehill and Ono 2012; Ono et al., 2013; Masterson 2011; Baroni et al., 2008).

Watanabe et al., (2009) reported chrome reducible organically associated polysulfides (CrS) from the thermochemical reduction of sulfate by glycine at temperatures between 150 and 200°C with positive $\Delta^{33}S$ values up to 2.1‰. This demonstrated an alternative geologic process could create MIF-S and explain correlations between MIF-S and characteristics of sediment. However these results did not conclusively provide evidence of a fractionation mechanism showing when or how MIF-S was created during TSR or showed how sulfate could be fractionated. Therefore the effects of TSR on MIF-S

signatures needs to be experimentally determined if its influence in the Archean is to be successfully refined.

1.2 Mechanism of MIF-S creation during TSR

Oduro et al. (2011) published the results of a series of TSR experiments with glycine and sodium sulfate at temperatures between 258^OC and 298^OC. Large enrichments of ^{33}S relative to ^{34}S and ^{36}S in residual polysulfide-chrome extractible sulfides relative to H_2S were reported. This discrepancy in the isotopic composition of the reduced sulfur products of TSR has been attributed to the magnetic isotope effect whereby the nuclear magnetic moment of isotopes with odd numbered atomic masses allow for hyperfine coupling in reactions during the reduction processes. This occurs during a spin selective reaction pathway during TSR that creates a sulfur ion pair radical, RSH*/RSSH, separate from the main reduction pathways responsible for H_2S creation. The products of this reaction, RSSSR, will show positive $\Delta^{33}S$ values while incurring no $\Delta^{36}S$ fractionation. Trends of large $\Delta^{36}/\Delta^{33}S$ ratios in H_2S can then be attributed to mass dependent fractionations of ^{36}S (Ono et al., 2006, Farquhar et. al., 2007). If the magnetic isotope effect alone is the only mechanism capable of creating MIF-S in TSR then it is not sufficient to create the fractionation trends observed in many Archean sulfides ($\Delta^{33}S/\delta^{34}S=1$, $\Delta^{36}S/\Delta^{33}S= -.8$). Further since the proposed reaction for this mechanism occurs after the formation of thiols it is not likely to mass independently fractionate sulfate.

MIF-S may also be generated by low activation energy reactions during a specific step of TSR. Lasaga et al. (2008) describe the mechanism behind this computationally where discrete differences in the vibrational energies of sulfur isopologues may cause discontinuities in the number of bound states within the potential well for a given reaction. The discontinuities occur between light and heavy isotopologues since the former is preferentially unbound due to its higher vibrational energy. This is shown schematically in figure 1 where a discontinuity is shown between the bond number of ^{32}S (n=4) and all

other sulfur isotopes (n=5) thus causing equal fractionations (fractionation slopes equal to one) in all $\delta^x S$ values. As a result mass independent enrichments in ^{33}S (positive $\Delta^{33}S$) and ^{36}S (negative $\Delta^{36}S$) occur as well as positive $\delta^{34}S$ fractionations in molecules that enter the reaction. A discontinuity between ^{33}S and ^{34}S would instead create mass independent depletions in ^{33}S while a discontinuity between ^{34}S and ^{33}S would create no $\Delta^{33}S$ fractionation but positive $\Delta^{36}S$ values. Here we refer to this mechanism as the vibrational energy discontinuity effect or VEDE. Lasaga et al modeled this phenomenon to simulate MIF-S creation during heterogeneous phase reactions (e.g. chemisorption reactions) since the activation energy for sorption processes is typically less than 50 kj/mol and therefore the differences in energies of the highest bound energy level would be greater as to increase the likelihood of bond discontinuities. Temperature is predicted to increase the magnitude MIF-S by increasing the energy potential of sulfur molecules giving a larger distribution at the highest bound level in the where discontinuities may potentially occur. Temperature however would also decrease the $\delta^{34}S$ fractionation resulting from this reaction much the same way it does through other isotope effects. Increased temperature thus increases the fractionation slope or λ ($\delta^{33}S_{Product}$-$\delta^{33}S_{Initial}$/ $\delta^{34}S_{Product}$-$\delta^{34}S_{Initial}$) values for ^{32}S discontinuities and decreases λ values for ^{33}S discontinuities. If VEDE occurs in an early stage of TSR then sulfate will be the residual product and thus possess opposite fractionations as sulfur that gets reduced by TSR.
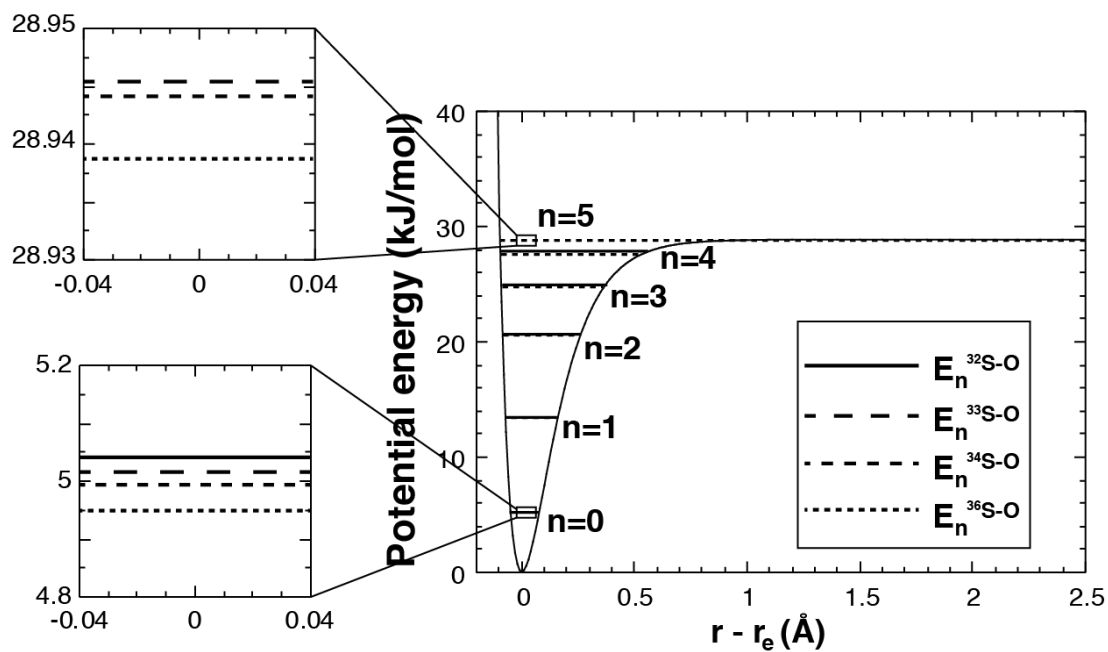
Figure 1: Morse Potential Schematic for MIF-S Creation by the Vibrational Energy Discontinuity Effect.

Potential energy for hypothetic S-0 interaction as a function of atomic distance for different sulfur isotopologues. Notice how bond number 5 is missing for ^{32}S due to the energy of dissociation for this reactions. Adopted from Lasaga et. al., 2008.

1.3 Objectives

Our goal is to determine how TSR fractionates S isotopes between sulfide and sulfate so that we may evaluate its relevancy in creating the MIF-S signatures in the Archean record as well as to improve the understanding of abiotic sulfur-carbon interactions. In order to do this we will identify the different isotope effects and fractionation processes during TSR. We will also investigate the influence of environmental parameters on the isotopic results of TSR by finding how different variables effects fractionation trends and magnitudes. This will be done by running TSR experiments at variety of conditions which will enable us analyze how these variables effect results. It will also allow us adjust reduction rates to produce the necessary amount of sulfur products to evaluate fractionations between H_2S, other sulfide species, and sulfate.

2. *Methods*

2.1. Starting Materials

Glycine (melting temperature = 233^OC) or a one to one mass ratio of glycine and alanine (melting temperature = 207^OC) were used in experiments to reduce sulfate. Crystalline amino acids along with sodium sulfate crystals provided by GFS Chemicals were added to the reaction vessel and dissolved with injected deionized oxygen purged water at the start of each experiment. At no point in any experiments were amino acid crystals completely dissolved. Sulfuric acid used in experiments was assayed at 95.6% H_2SO_4 by Baker Intra-Analyzed Reagent and mixed with amino acids before entering the reaction vessel. Prior to Hydrous H_2SO_4 experiments water was added in the same manner as sodium sulfate experiments. Conditions of experiments carried out in this study are summarized in table 1.

2.2. Experimental Set up and procedure

We used the same open system experimental apparatus that was utilized in experiments conducted by Watanabe et al 2009. A schematic illustration can be found in supplemental figure 1. Temperatures of reaction vessels were maintained by thermocouples attached to heating mantles. H_2S was collected in zinc acetate traps that were changed once adequate amounts of ZnS were recovered for isotope analysis (usually at least 2mg once converted to Ag_2S). All experiments were carried out until H_2S production ceased determined by the ability of outflowing gas to reduce Ag_2NO_3.

2.3. Post Experiment Analysis

Once experiments stopped producing H_2S the individual collections of Ag_2S were weighed and analyzed for sulfur content using CE instruments NC2500 elemental analyzer. The duration of an individual collection and its sulfur yield was used to determine H_2S production rate. A three step sequential extraction utilizing H_2O, HCl and Cr-solution (Canfield et al., 1986) was employed to collect sulfur bearing species from residual solids left in the reaction vessels. At the conclusion of some experiments yellow S^0 had precipitated in the top half of the reaction vessel. This was extracted from the vessel using Cr-Solution once the residual solid was removed. Water dissolvable sulfur was precipitated with $BaCl_2$ to collect sulfate as $BaSO_4$ or sulfite as $BaSO_3$. These were then analyzed using the elemental analyzer to determine residual, non reduced sulfate amounts and extracted using Thode solution (Thode et al., 1961). Amounts of HCl dissolvable sulfur (HClS) and chromium reducible sulfur (CrS) were determined through mass measurement and elemental analysis of Ag_2S. Extracted S^0 amounts are reported however some amounts of volatized sulfur may be carried out the experimental apparatus by carrier gas. A schematic illustration showing the sequence collection of sulfur from experiments is provided in supplemental figure 2.

2.4. Isotopic Analysis

Ag_2S samples were loaded in nickel reaction tubes and reacted with F_2 gas at 275^OC for 12 hours to generate SF_6. Samples were then purified through a manifold consisting of cryogenic traps and a gas chromatograph for purification before being introduced to a VG Prism mass spectrometer for ^{32}S, ^{33}S, and ^{34}S at Penn State. International sulfur isotope standard S1 was analyzed once for every 3 to 5 experimental samples to monitor accuracy and precision. IAEA-S-1 $\delta^{34}S$ and $\Delta^{33}S$ measurements were between +/- .2 and .02 per mil respectively relative to PSU standard gas ($R_{34S/32S}$= .0446, $R_{33/32}$= .00792, $R_{36/32}$= .000213). Selected samples including initial experimental sulfates were taken to the University of Maryland for ^{36}S analysis in the fall of 2011 and spring of 2013. All Isotope values are reported in δ notation relative to initial experimental sulfates (δ^XS=(R_{Sample}/R_{STD}-1)*1000. Thode solution extracted GFS sodium sulfate and Backer sulfuric acid we analyzed several times over the course isotopic analysis. $\Delta^{33}S$ and $\Delta^{33}S$ values are calculated using linear mass dependent slopes of .515 and 1.89 respectively which have been described as suitable for describing the equilibrium exchange at high temperatures for reactions involving H_2S and sulfate by Otake et al. 2008.

3. Results

3.1. Trends in Products of TSR by experiment type

Summaries of experimental yields of different extractable sulfur species relative to initial sulfur amounts are provided in table 1. Reduction amounts vary most by initial sulfur type. The highest H_2S yields come from sulfuric acid experiments. Roughly three orders of magnitude more H_2S was produced when sodium sulfite was reduced as opposed to sodium sulfate using glycine at 150^OC. From experiments with sodium sulfate the highest H_2S yields come from those with alanine while experiments run at 200^OC with glycine and amino acid mixtures produce roughly the same amount of H_2S. Mixture and glycine experiments also produce roughly the same amount of total reduced sulfur in A.H_2SO_4 experiments however in glycine experiments most is collected as CrS as opposed to H_2S. Low

temperature glycine and sodium sulfate experiments produced approximately an order of magnitude less than experiments at 170 and 200°C. No CrS was present in 200°C glycine or mixture sodium sulfate experiments but was extracted at lower and higher temperatures. In both mixture and glycine sulfuric acid series as temperature increased from 200°C to 250°C so did the total reduced sulfur by roughly 200% to 300% as well as the relative amount of H$_2$S to CrS. Higher temperature acid experiments also left less water soluble residual sulfate. None recovered sulfur likely represents volatized species (sulfate aerosols, SO$_2$, S^0) that were not collected in the zinc acetate traps.

ID	Analyst	Amino Acids	Sulfur Source	Run T (^oC)	Run Duration (hrs)	% H_2S	% Cr-S	% HCl-S	% S^0	% Reduced$_{Total}$	% $SO_4^{2-}{}_{Residual}$	% Non Recovered
A-SSI-150-1	1	Alanine	Na_2SO_3	150	24.83	11.04	NR	NR	NR	11.04	NM	NM
G-SSI-150-1	1	Glycine	Na_2SO_3	150	24.83	6.98	NR	NR	NR	6.98	NM	NM
G-SSI-150-2	1	Glycine	Na_2SO_3	150	23.83	2.25	NR	NR	NR	2.25	NM	NM
A-SSA-180-1	1	Alanine	Na_2SO_4	150-180	46	1.02	NM	NR	NR	NM	75.69	NM
G-SSA-180-1	1	Glycine	Na_2SO_4	150-180	36.1	0.25	0.03	NR	NR	0.28	75.84	23.88
G-SSA-170-1	1	Glycine	Na_2SO_4	170	480.5	1.03	NM	NR	NR	NM	85.76	NM
G-SSA-170-2	1	Glycine	Na_2SO_4	170	480.5	0.51	NM	NR	NR	NM	93.58	NM
G-SSA-150-1	1	Glycine	Na_2SO_4	150-160	1897.5	0.03	IS	NR	NR	0.03	56.48	99.97
G-SSA-150-2	1	Glycine	Na_2SO_4	150-160	1273	0.05	NM	NR	NR	NM	95.91	NM
G-SSA-150-3	1	Glycine	Na_2SO_4	150-160	1273	0.01	NM	NR	NR	NM	94.05	NM
G-SSA-200-1	1	Glycine	Na_2SO_4	200	265	0.63	NR	NR	NR	0.63	90.59	8.78
G-SSA-200-2	1	Glycine	Na_2SO_4	200	265	0.26	NR	NR	NR	0.26	79.00	20.74
G-SSA-200-3	1	Glycine	Na_2SO_4	200	3	0.30	NR	NR	NR	0.30	NM	NM
M-SSA-200-1	3	Mix	Na_2SO_4	200	3	0.09	NR	NR	NR	0.09	NM	NM
M-SSA-200-2	3	Mix	Na_2SO_4	200	3	0.14	NR	NR	NR	0.14	NM	NM
M-SSA-200-3	3	Mix	Na_2SO_4	200	10	0.16	NR	NR	NR	0.16	80.82	19.02
M-SSA-200-4	3	Mix	Na_2SO_4	200	48	0.80	NR	NR	NR	0.80	99.08	0.12
G-HSA-300-1	3	Glycine	H. H_2SO_4	300	3	40.93	NR	NR	NR	40.93	NR	59.07
G-HSA-200-1	3	Glycine	H. H_2SO_4	200	107.5	17.47	7.17	NR	NR	24.64	NR	75.36
G-ASA-200-1	3	Glycine	A. H_2SO_4	200	96	NR	7.48	NR	NR	7.48	3.08	89.44
G-ASA-200-2	3	Glycine	A. H_2SO_4	200	49	NR	0.42	NR	NR	0.42	39.02	60.56
G-ASA-200-3	3	Glycine	A. H_2SO_4	200	49	NR	12.14	NR	NR	12.14	10.75	77.11
G-ASA-250-1	3	Glycine	A. H_2SO_4	250	49	0.95	27.50	NR	4.38	32.83	3.30	63.87
M-ASA-250-1	3	Mix	A. H_2SO_4	250	57.5	29.46	2.04	2.99	1.64	36.13	8.72	55.15
M-ASA-250-2	3	Mix	A. H_2SO_4	250	57.5	34.92	1.86	1.22	2.94	40.94	9.30	49.76
M-ASA-200-1	3	Mix	A. H_2SO_4	200	23.5	3.26	8.74	0.92	0.89	13.81	30.33	55.86
G-SSA-258-1	2	Glycine	Na_2SO_4	258	340	NM	NM	NR	NR	NM	NM	NM
G-SSA-298-1	2	Glycine	Na_2SO_4	298	340	NM	NM	NR	NR	NM	NM	NM

Table 1: Summary of Experiment Details and Product Yields.

Column labels 1, 2, and 3 under Analyst indicate experiment results published in Watanabe at al., 2009, Oduro et. al., 2011, and this study respectively. Abbreviations H. and A. under sulfur source indicate hydrous or anhydrous H_2SO_4. Percent values refer to the final fraction of initial oxidized sulfur converted to the specific sulfur product labeled for each column. Please refer to Supplemental Table 1 for initial sulfur amounts. Cells labeled NM and NR stand for not measured and not recovered products respectively. Not measured products were present at the conclusion of the experiment and often analyzed for isotopic composition however their amount was not measured. Experimental conditions are summarized in the ID column and will be used as labels for individual experiments in proceeding text and tables. ID labels are separated into four components. The first component abbreviates the amino acid type, the second abbreviates the sulfur source (SSI for sodium sulfite, SSA for sodium sulfate, HAS for hydrous sulfuric acid, and ASA for anhydrous sodium sulfate), the third component gives the approximate experimental temperature, and the last component gives the run number for a specific condition indicated in the first three components.

3.2. Isotope Results

The isotopic compositions of TSR products are summarized in table 1. A complete data set is presented in supplemental table 1. Individual H_2S collected cover a $\delta^{34}S$ range from -20 to 15‰ with a largely unimodal distribution around -5‰ per mil while bulk H_2S collected from individual experiments range from -15 to 6‰. $\Delta^{33}S$ values of H_2S are largely positive with fractionation up to 2.3‰. Negative $\Delta^{33}S$ fractionations are observed in H_2S collected at the end of M-ASA experiments. The $\delta^{34}S$ range of CrS is narrower than that of H_2S with values between -15.81 and 5.59‰ however they contain higher $\Delta^{33}S$ fractionations with values up to 13.55‰ for higher temperature experiments performed by Oduro et al. Residual sulfate contain largely positive $\delta^{34}S$ and negative $\Delta^{33}S$ values with the largest fractionations coming from anhydrous sulfuric acid experiments. Fractionation trends, quantified with λ ($\lambda = (\delta^{33}S_{product} - \delta^{33}S_{Initial})/(\delta^{34}S_{product} - \delta^{34}S_{Initial})$) are measured above and below the mass dependent fractionation line with a range of .199 to 2.618 for MIF-S containing H_2S and -8.459 to 1.373 for CrS. The following sections will go into extensive coverage of results by experiment type and fractionation between different sulfur species.

ID	$\delta^{34}S$ (‰) H2S Range	$\delta^{34}S$ (‰) H2S Bulk	$\delta^{34}S$ (‰) Cr-S	$\delta^{34}S$ (‰) HCl-S	$\delta^{34}S$ (‰) S^0	$\delta^{34}S$ (‰) Reduced total	$\delta^{34}S$ (‰) SO_4^{2-} Residual	$\Delta^{33}S$ (‰) H2S Range	$\Delta^{33}S$ (‰) H2S Bulk	$\Delta^{33}S$ (‰) Cr-S	$\Delta^{33}S$ (‰) HCl-S	$\Delta^{33}S$ (‰) S^0	$\Delta^{33}S$ (‰) Reduced total	$\Delta^{33}S$ (‰) SO_4^{2-} Residual	λ H2S Range	λ H2S Bulk	λ Cr-S
A-SSI-150-1	.71 to 4.06	3.09	--	--	--	3.09	--	-.07 to .02	-0.01	-0.01	--	--	-0.01	--	.095 to .545	0.511	--
G-SSI-150-1	-4.67 to 2.29	-1.24	-1.24	--	--	-1.24	--	-.06 to .04	-0.01	-0.01	--	--	-0.01	--	.504 to .533	0.519	--
G-SSI-150-2	-4.11 to 1.34	-0.6	-0.6	--	--	-0.6	--	-.08 to 0	-0.04	-0.04	--	--	-0.04	--	.485 to .556	0.588	--
A-SSA-180-1	-5.23 to .89	-1.89	0.592	--	--	--	0.08	.05 to .13	0.07	0.07	0	--	--	-0.03	-.15 to .58	0.476	0.515
G-SSA-180-1	-6.93 to -2.37	-4.08	-9.881	--	--	-4.697	-0.06	.09 to .22	0.14	0.14	-0.06	--	0.12	-0.01	.472 to .496	0.481	0.521
G-SSA-170-1	-6.51 to -3.34	-5.03	1.76	--	--	--	0.26	.1 to .38	0.25	0.25	0.57	--	--	-0.01	.402 to .490	0.466	0.839
G-SSA-170-2	-2.62 to 4.98	-0.71	2.4	--	--	--	0.06	.17 to .37	0.31	0.31	2.06	--	--	-0.02	.199 to .686	0.086	1.373
G-SSA-150-1	-11.42 to -9.00	-10.08	-7.95	--	--	-10.08	--	.26 to .48	0.36	0.36	-0.06	--	0.35	--	.473 to .486	0.479	0.523
G-SSA-150-2	-20.82 to -12.88	-15.89	-5.36	--	--	--	--	.17 to .56	0.35	0.35	0.2	--	--	--	.472 to .505	0.491	0.478
G-SSA-150-3	-13.67	-13.67	-6.49	--	--	--	--	.231	0.23	0.23	0.04	--	--	--	.498	0.498	0.509
G-SSA-200-1	-11.37 to -4.98	-6.21	--	--	--	-6.21	--	.33 to .58	0.43	0.43	--	--	0.43	--	.398 to .467	0.445	--
G-SSA-200-2	-4.63	-4.63	--	--	--	-4.63	--	.925	0.925	0.925	--	--	0.925	--	.315	0.315	--
G-SSA-200-3	-6.22 to -5.3	-5.82	--	--	--	-5.82	--	.58 to .89	0.76	0.76	--	--	0.76	--	.371 to .405	0.385	--
M-SSA-200-1	-9.53	-9.53	--	--	--	-9.53	4.28	2.21	2.21	2.21	--	--	2.21	-0.07	.283	0.283	--
M-SSA-200-2	-10.58 to -5.87	-8.64	--	--	--	-8.64	-0.27	2.08 to 2.3	2.21	2.21	--	--	2.21	0	.158 to .298	0.259	--
M-SSA-200-3	-7.69 to -7.32	-7.46	--	--	--	-7.46	3.48	1.53 to 2.2	1.78	1.78	--	--	1.78	-0.09	.229 to .305	0.277	--
M-SSA-200-4	.89 to 15.5	5.4	--	--	--	5.4	0.37	.48 to 1.87	1.2	1.2	--	--	1.2	0	.546 to 2.618	0.739	--
G-HSA-300-1	-2.35 to -10.28	-2.64	--	--	--	-2.64	--	-.02 to .07	-0.02	-0.02	--	--	--	--	.508 to .523	0.521	--
G-HSA-200-1	-9.75 to -3.41	-5.31	0.26	--	--	-3.69	--	.06 to .1	0.08	0.08	0.07	--	0.08	--	.495 to .507	0.499	0.784
G-ASA-200-1	--	--	-15.47	--	--	-15.47	3.08	--	--	--	0.2	--	0.2	-0.01	--	--	0.502
G-ASA-200-2	--	--	--	--	--	--	1.71	--	--	--	--	--	--	0.01	--	--	
G-ASA-200-3	-8.73	--	-8.73	--	--	-8.73	5.65	--	--	0.14	0.14	--	0.14	-0.02	--	--	0.499
G-ASA-250-1	-8.85	-8.85	-5.51	--	-2.13	-5.16	7.85	.08	0.08	0.08	0.1	0.12	0.1	-0.15	.506	0.506	0.497
M-ASA-250-1	-9.9 to 2.35	-4.89	5.3	5.6	-1.04	-3.07	3.3	-.22 to .21	0.12	0.12	-0.08	0.16	0.06	0.09	.335 to .483	0.49	0.500
M-ASA-250-2	-7.94 to 1.58	-4.26	5.59	6.64	-0.57	-2.88	3.85	-.21 to .17	0.1	0.1	-0.09	0.13	0.08	0.09	.376 to .592	0.491	0.499
M-ASA-200-1	-12.14 to -13.14	-12.72	-4.44	-4.85	-6.15	-6.53	6.64	.08 to .1	0.09	0.09	0.14	0.11	0.12	0.06	.506 to .508	0.508	0.483
G-SSA-258-1	-19.21	-19.21	-15.81	--	--	--	-8.12	.18	0.18	0.18	2.75	--	--	0.01	.505	0.505	0.341
G-SSA-298-1	-9.93	-9.93	-1.51	--	--	--	0.91	1.17	1.17	13.55	--	--	--	-0.03	.397	0.397	-8.459

Table 2: Summary of Isotopic Data

All values normalized to $\delta^{33}S$ and $\delta^{34}S$ values of zero for initial sulfur. Measured H_2S ranges and calculated bulk H2S values from the mass normalized summation of measured samples for each experiment are provided. For Individual H2S isotope data and amount refer to Supplemental Table 1. Reduced Total isotope data is calculated based the isotopic composition of H2S, CrS, HClS, and S^0 and their relative abundances provided in table 1. Bolded λ values indicate samples with $\Delta^{33}S$ values below .20‰.

3.2.1. Results of Glycine Experiments

G-SSI-150

Figure 2a. contains $\delta^{34}S$ and $\Delta^{33}S$ data for all H_2S and sulfate collected during experiments between glycine and various oxidized sulfur species. H_2S produced from Experiments run with sodium sulfite at 150°C are circled in orange. These samples contain relatively small isotope fractionations with a $\delta^{34}S$ range from -4.67 to 2.29 ‰, bulk value of -1.24 and -.60‰, and no MIF-S $\Delta^{33}S$ values.

G-SSA-150

Experiments run at 150 to 160°C with sodium sulfate produced H_2S with a $\delta^{34}S$ range from -20.82 to -9.00‰ and mostly mass independent $\Delta^{33}S$ values between 0.18 and 0.56‰. These samples are grouped in the blue bubble and possess λ values below the mass dependent line from .473 to .505. Multiple $\Delta^{33}S$ values fall along similar λ trends but, as noted in figure 2a., the sample with the highest lambda has the lowest $\Delta^{33}S$ value while the sample with the lowest lambda has the highest $\Delta^{33}S$ value. As described as a fractionation amongst H_2S for this series, this observation can be said to exhibit a positive $\Delta^{33}S_{H2S-H2S}/\Delta^{34}S_{H2S-H2S}$ trend.

G-SSA-170

Experiments run at 170°C are noticeable heavier than lower temperature results with a $\delta^{34}S$ range between -5.3 and 4.98‰. Although positive $\delta^{34}S$ values from initial sulfate are observed in some samples, bulk H_2S values for experiments run at these conditions are -5.03 and -0.71‰. $\Delta^{33}S$ values range between 0.17 and 0.38‰ and are similar to those measured in 150°C experiments. The λ values deviate further than lower temperature experiments both below the mass dependent range, $\lambda_{min}= 0.192$, and above it, $\lambda_{max}=0.683$.

Figure 2b shows how λ and $\Delta^{33}S$ of H_2S changes through run time for two of these experiments. The fractionation trend increases then decreases then increases again over the course of experiment G-SSA-170-1 going above and below the mass dependent trend. Interestingly when λ

goes from below to above the mass dependent line, the $\Delta^{33}S$ values go down and when the opposite occurs $\Delta^{33}S$ goes up. This negative correlation between $\delta^{34}S$ and $\Delta^{33}S$ of H_2S observed through a single experiment is similar to that observed in 150°C series which contains a positive $\Delta^{33}S_{H2S-H2S}/\Delta^{34}S_{H2S-H2S}$. Experiment G-SSA-170-2 shows much more consistent fractionation trends all below the mass dependent line between .402 and .486 however, the range of $\Delta^{33}S$ values is similar to experiment G-SSA-170-1, .19 to .37‰ and .17 to .38‰ respectively.   Like experiment G-SSA-170-1, the same negative correlation between lambda change and $\Delta^{33}S$ change is observed, except where lambda is initially increasing for experiment G-SSA-170-1, here it decreases from .486 to .401 from hours 47.5 to 118.5 and $\Delta^{33}S$ increases from .15 to .378.

G-SSA-200

The $\delta^{34}S$ range of 200°C experiments, -11.37 to -4.43‰, overlaps with lighter values of 150°C and heavier values of 170°C series. However the $\Delta^{33}S$ range and maximum are greater, .33 to .93‰, than either lower temperature series. λ values are between .467 and .315, which places them with in the range of 170°C experiments, and lower than the range of the 150°C series. As noted during 170°C series, λ values and $\Delta^{33}S$ fractionation have a negative correlation during these experiments. Also a positive $\Delta^{33}S_{H2S-H2S}/\Delta^{34}S_{H2S-H2S}$ trend is also observed as samples with the lowest λ and highest $\delta^{34}S$ values contain the highest $\Delta^{33}S$ fractionation.

The minimum $\delta^{34}S$ values of G-SSA experiments are very similar to the kinetic isotope fractionations of -15‰ at 150°C and -10‰ at 200°C for TSR compiled by Machel, Krouse, and Sassen 1995.

G-SSA-258+298

H_2S from experiments above 250^{0}C with Sodium sulfate and glycine run by Oduro et. al. show the highest range and degree of mass independent fractionation ($\Delta^{33}S$= .18‰ for 258°C and 1.17‰ for 298°C) as well as the highest range $\delta^{34}S$ fractionation, $\delta^{34}S$ from -15.81 to -1.51‰. Correlation between $\Delta^{33}S$ and $\delta^{34}S$ fractionation also creates another positive $\Delta^{33}S_{H2S-H2S}/\Delta^{34}S_{H2S-H2S}$

trend over a λ range between .505 and .397.

G-ASA+HSA

Glycine and sulfuric acid experiments run above 200°C show no mass independent fractionation but positive Δ^{33}S values. The extent of mass dependent fractionation in these runs is very similar to 200°C sodium sulfate experiments with a Δ^{33}S range from -9.75 to -3.01‰. Residual sulfate from these experiments show positive δ^{34}S values up 7.85‰ and negative Δ^{33}S values with a maximum fractionation of -.15‰. Detailed discussion on the fractionation between sulfate and reduced sulfur will be discussed in latter section 3.2.4.
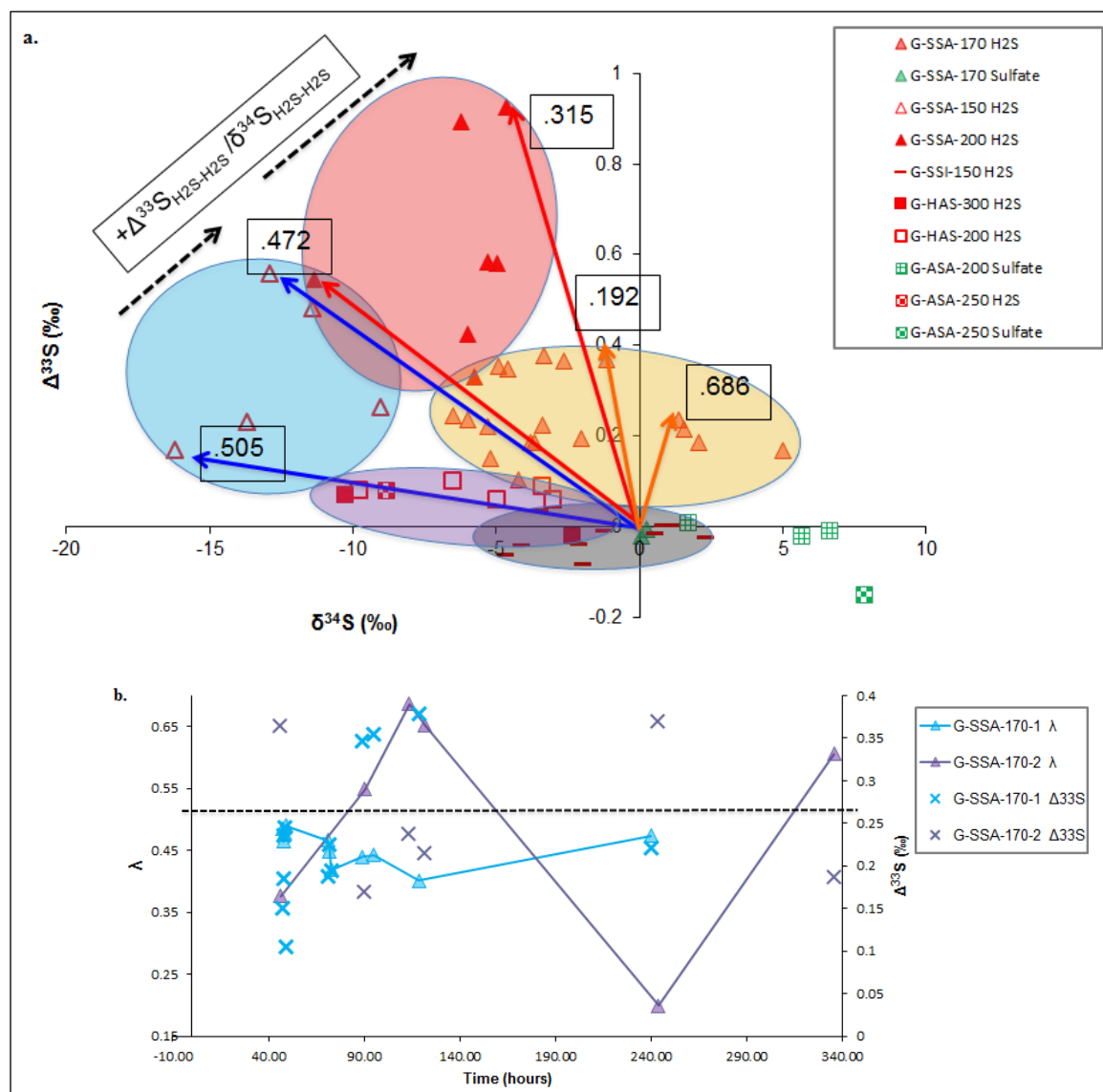
Figure 2. Isotope data of H₂S and Sulfate from Glycine experiments

Red, orange, and blue shaded ovals represent isotope values of H₂S from G-SSA-200, G-SSA-170, and G-SSA-150 experiments respectively in (a). λ values for experiments are indicated with corresponding colored arrows and black text boxes. Black arrows show fractionation trends of H₂S. Experiments using acid and sulfite as a sulfur source are highlighted with the purple and black ovals respectively. In (b). isotope results of individual H₂S collections through time for G-SSA-170 experiments. Connected triangles show trends in λ indicated on the left axis while X's show changes $\Delta^{33}S$ over time.

3.2.2. Isotope results of mix amino acid experiments

M-SSA-200

Mixture amino acid experiments with sodium sulfate run at 200^OC cover the largest mass dependent range of any experimental series. δ^{34}S values are as heavy as 15.5‰ and as light as -9.53‰. Δ^{33}S values range from 0.48 to 2.30‰. The magnitude and range of mass independent fractionation is greater than any other experimental series. λ values, labeled on figure 3a., extend further above and below the mass dependent line than any other series. Also labeled is the Δ^{33}S$_{H2S\text{-}H2S}$/Δ^{34}S$_{H2S\text{-}H2S,}$ slope which unlike series with glycine a sodium sulfate, is negative. This trend is independent of lambda value as the correlation between lower δ^{34}S values and higher Δ^{33}S values is observed as lambda goes from infinitely positive to infinitely negative.   However, as observed along λ=.305 in the figure 3a., samples of varying Δ^{33}S values may fall on the same fractionation trend.

The δ^{34}S range of individual M-SSA experiments falls with in either positive or negative values. Experiment M-SSA-200-4 contains all positive fractionated samples with a bulk isotopic composition of 5.38‰. This experiment also contains the largest amount of reduced (.8%) and recovered sulfur. Experiment M-SSA-200-1 contains the most depleted fractionations, δ^{34}S= -9.53‰, and the smallest amount of reduced sulfur (.08%). As observed G-SS-170-1, trends in λ values are inconsistent over the duration of experiment M-SSA-200-4. The initial increase then decrease of λ over time correlate with increases and decreases in Δ^{33}S values.

G-ASA-200+250

No mass independent fractionation is observed in H_2S from the M-ASA-200 experiment although this experiment exhibits the most negative mass dependent fractionation of any mixture amino acid series (δ^{34}S= -12.14 and -13.14‰). 250^OC experiments exhibit both positive and negative mass independent (Δ^{33}S= -.22 to .21‰) and dependent fractionation (δ^{34}S from -9.90 to 2.34‰) For both these experiments the change from positive to negative Δ^{33}S and negative to positive δ^{34}S direction roughly correlate with time and match one and other.

Residual sulfate exhibit positive mass dependent fractionation in both sodium sulfate, $\delta^{34}S_{Max}=$ 4.28‰, and H_2SO_4 experiments, $\delta^{34}S_{Max}=$ 6.64‰, with negative $\Delta^{33}S$ values. Detailed discussion on relative sulfate and reduced sulfur fractionation will follow in section 3.2.4

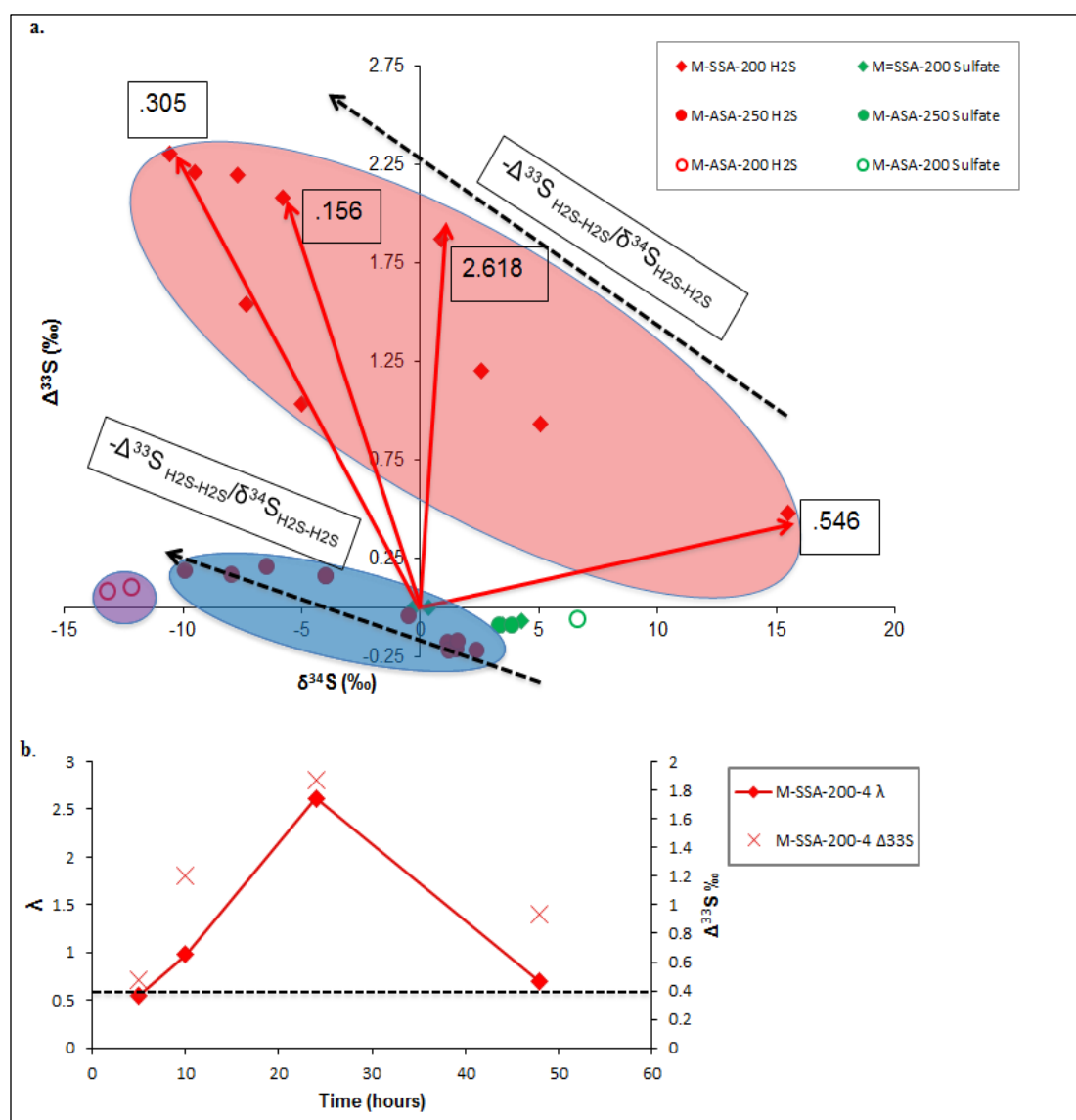*Figure 3. Isotope data of H₂S and sulfate from mixture amino acid experiments*

Red, blue, and purple show the regions of individual H₂S from M-SSA-200, M-ASA-250, M-ASA-200 experiments respectively with corresponding colored arrows to show lambda values. Black arrows indicate trends in H₂S fractionation. Changes in λ (connected triangles) and Δ³³S (X's) over the course of experiment M-SSA-200-4 shown in b.

3.2.3. Isotopic Results of Alanine Experiments

Experiments with alanine and sodium sulfite at 150^OC produce H_2S with near zero $\Delta^{33}S$ values and positive $\delta^{34}S$ fractionation between from .71 and 4.06‰. Sodium sulfate experiments at 150-180°C (which contained less total reduced sulfur) contained positive $\Delta^{33}S$ values but no mass independent fractionation. $\delta^{34}S$ values were largely negative ranging between -5.23 and .892‰ with a cumulative value of -1.89‰.
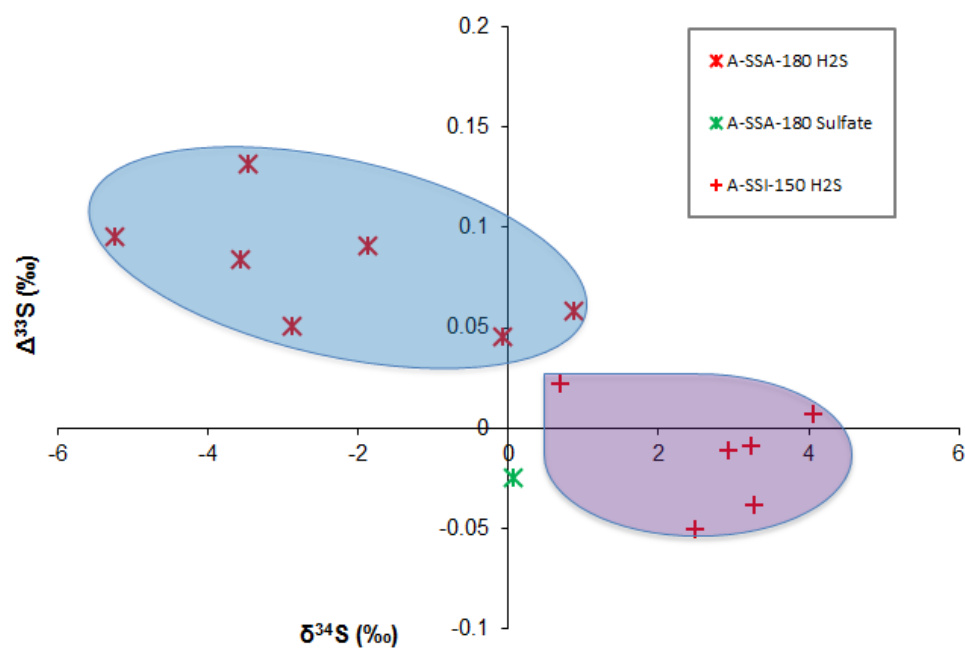
Figure 4. Isotope data of H$_2$S from alanine experiments

Experiments with sodium sulfate and sodium sulfite circled in blue and purple respectively.

ID	$\Delta^{34}S_{H2SB\text{-}Sulfate}$	$\Delta^{33}S_{H2SB\text{-}Sulfate}$	$\Delta^{34}S_{CrS\text{-}Sulfate}$	$\Delta^{33}S_{CrS\text{-}Sulfate}$	$\Delta^{34}S_{H2SF=CrS}$	$\Delta^{33}S_{H2SF\text{-}CrS}$	$\Delta^{34}S_{H2SF\text{-}HClS}$	$\Delta^{34}S_{H2SB\text{-}S0}$
A-SSA-180-1	-1.97	0.10	-0.67	0.03	-2.87	0.13	--	--
G-SSA-180-1	-4.02	0.15	-9.82	-0.05	7.51	0.16	--	--
G-SSA-170-1	-5.29	0.25	1.50	0.57	-7.05	-0.35	--	--
G-SSA-170-2	-0.77	0.32	2.34	2.08	-0.34	-1.87	--	--
G-SSA-150-1	--	--	--	--	-1.06	0.32	--	--
G-SSA-150-2	--	--	--	--	-15.46	-0.03	--	--
G-SSA-150-3	--	--	--	--	-7.18	0.19	--	--
M-SSA-200-1	-13.81	2.28	--	--	--	--	--	--
M-SSA-200-2	-8.37	2.21	--	--	--	--	--	--
M-SSA-200-3	-10.94	1.87	--	--	--	--	--	--
M-SSA-200-4	5.01	1.20	--	--	--	--	--	--
G-HSA-200-1	--	--	--	--	-5.24	-0.01	--	--
G-ASA-200-1	--	--	-22.08	0.21	--	--	--	--
G-ASA-200-3	--	--	-14.38	0.16	--	--	--	--
G-ASA-250-1	-16.70	0.23	-13.36	0.25	-3.34	-0.02	--	-6.72
M-ASA-250-1	-8.19	0.21	2.00	0.01	-4.08	-0.14	-4.38	-3.85
M-ASA-250-2	-8.11	0.19	1.74	0.00	-4.01	-0.08	-5.06	-3.69
M-ASA-200-1	-19.36	0.15	-11.08	0.20	-8.29	-0.06	-8.29	-6.57
G-SSA-258-1	-11.09	0.17	-7.69	2.74	-3.40	-2.57	--	--
G-SSA-298-1	-10.84	1.20	-2.42	13.58	-8.42	-12.38	--	--

Table 3: Sulfur Species Fractionation from TSR

Differences in isotopic composition between various sulfur bearing TSR products reported for

$^{34}S/^{32}S$ ($\Delta^{34}S$) and $\Delta^{33}S$ fractionations.

3.2.4. Fractionation of sulfur species

3.2.4.1 Fractionation between sulfate and H$_2$S$_{Bulk}$

Fractionation between residual sulfate and bulk H$_2$S summarized in table 3 varies considerably.

Δ^{34}S$_{H2SB-Sulfate}$ fractionations ranges from -16.70 to 5.01‰ however are largely negative. Δ^{33}S$_{H2SB-Sulfate}$

fractionations are always positive ranging from 0 .1 to 2.28‰. Values also vary considerably by

experiment condition. The range of mass dependent fractionation for M-SSA-200 experiments varies

from -13.81 to 5.01‰ and 2.28 to 1.20‰ for mass independent fractionation. Sodium sulfate and glycine

experiments run at 170°C have Δ^{34}S$_{H2SB-Sulfate}$ values of -5.29 and -.77‰ for G-SSA-170-1 and G-SSA-

170-2 respectively. However for this series as well as mixture and H$_2$SO$_4$ (Δ^{34}S$_{H2B-Sulfate}$ range of -8.11 to

-19.36‰) and glycine and sodium sulfate at temperatures above 250°C series, the experiments that had

smaller mass dependent fractionation between sulfate and H$_2$S$_{Bulk}$ had larger mass independent

fractionations.

Figure 5 shows the δ^{34}S and Δ^{33}S fractionations for residual sulfate and H$_2$S$_{Bulk}$ as function of the

H$_2$S to residual sulfate molar ratio at the end of an experiment. This ratio covers a range of over three

orders of magnitude from an H$_2$S$_{Bulk}$/SO$_4^{2-}$ of 1.93x10^{-3} for experiment M-SSA-200-3 to 2.66 for

experiment M-ASA-250-2. However the change in δ^{34}S of H$_2$S$_{Bulk}$ from the lowest to the highest H$_2$S

producing experiments is only 2.83‰. δ^{34}S$_{H2SB}$ initially increases for experiments with higher

H$_2$S$_{Bulk}$/SO$_4^{2-}$ ratios until M-SSA-200-4 which has heavier bulk total reduced sulfur than residual sulfate.

As the H$_2$S$_{Bulk}$/SO$_4^{2-}$ ratio increases from this experiment δ^{34}S and Δ^{34}S$_{Sulfate-H2SB}$, actually get lighter. In

fact with higher H$_2$S$_{Bulk}$/SO$_4^{2-}$ ratios G-SSA-170 experiments show lighter, more fractionated δ^{34}S$_{H2SB}$

values. Minimum δ^{34}S values for H$_2$S$_{Bulk}$ and maximum Δ^{34}S$_{Sulfate-H2SB}$ values are observed at a

H$_2$S$_{Bulk}$/SO$_4^{2-}$ ratio of 1.07x10^{-1} for the M-ASA-200 experiment. As H$_2$S$_{Bulk}$/SO$_4^{2-}$ ratios increase from

here Δ^{34}S values show less fractionation.

The δ^{34}S and Δ^{33}S values of residual sulfate do not differ from the lowest to highest H$_2$S

producing experiments. However the δ^{34}S values of residual sulfate was less than 0.5‰ for all

experiments but one with a H_2S_{Bulk}/SO_4^{2-} ratio less than 1.12×10^{-2}. All H_2SO_4 experiments with higher H_2S_{Bulk}/SO_4^{2-} ratios have heavy $\delta^{34}S$ values although the magnitude of fractionation, $\Delta^{34}S_{H2SB-Sulfate}$, decreases for the experiments with the greatest amount of relative H_2S production (G-ASA-250 to M-ASA-250). $\Delta^{33}S$ fractionation for residual sulfate follows the mass $\delta^{34}S$ trend where experiments with the most positive $\delta^{34}S$ values have the most negative $\Delta^{33}S$ regardless of H_2S_{Bulk}/SO_4^{2-} ratio.

The $\delta^{34}S$ trends for sulfate and H_2S_{Bulk} almost reflect each other so that the most negative fraction factors are observed when each is fractionated the most in the opposite direction. Exceptions to this relationship are observed between the two most fractionated experiments, G-ASA-250 and M-ASA-200, where the latter has more fractionated H_2S, a larger $\Delta^{34}S_{H2SB-Sulfate}$ value, but less fractionated residual sulfate, as well as experiment M-SSA-200-4 where H_2S_{Bulk} is actually heavier than the residual sulfate. The relative scaling of the mass dependent fractionation between sulfate and H_2S through H_2S_{Bulk}/SO_4^{2} ratio varies considerably. At H_2S_{Bulk}/SO_4^{2-} ratios less than one the $\delta^{34}S$ fractionation magnitude for H_2S_{Bulk} are always greater than residual sulfate and in the opposite direction, the exception again being M-SSA-200-4. Interestingly in M-ASA-250 experiments where the amount of H_2S produced exceeds the amount of residual sulfate by about 2.5 times, H_2S was still more fractionated. It is also shown that $\Delta^{33}S_{Sulfate-H2SB}$ fractionation does not scale in any matter with H_2S_{Bulk}/SO_4^{2-} ratios.

Figure 5. Relative H₂S to Sulfate Fractionation Comparison

$\delta^{34}S$ *of sulfate, solid green line, and* H_2S_{Bulk}*, solid red line as a function of final the ratio of* H_2S *to sulfate at the end of individual experiments plotted on the left axis.* $\Delta^{33}S$ *of sulfate, dotted green line, and* H_2S_{Bulk}*, dotted red line, are plotted on the right axis.* $\Delta^{34}S$ *and* $\Delta^{33}S$ *fractionations between species for each experiment can be inferred from the relative difference on the left and right axis for solid and dotted lines respectively. The black shaded oval indicates the experiment where* H_2S_{Bulk} *is heavier that sulfate. Symbols for experiments are the same as those indicated for figures 2 and 3.*

3.2.4.2 Cr-S and residual sulfate fractionation

Table 3 also contains fractionations between residual sulfate and Cr-S. $\Delta^{34}S_{CrS-Sulfate}$ values range

from -22.08 to 2.38‰ showing a similar amount of variation as $\Delta^{34}S_{H2SB-Sulfate}$. Positive fractionation

factors are observed in both G-SSA-170 and both M-ASA-250 experiments. Figure 6 shows the $\delta^{34}S$ and

$\Delta^{33}S$ fractionations for residual sulfate and CrS as function of $CrS/SO_4^{2-}{}_{Residual}$ molar ratio at the end of

experiments. $\delta^{34}S$ fractionation for CrS is largely independent of $CrS/SO_4^{2-}{}_{Residual}$ ratio. An increase in

$\delta^{34}S$ values of about 15‰ is observed as CrS/SO_4^{2-} increases by nearly three orders of magnitude from G-

SSA-180 experiments to M-ASA-250 experiments. CrS then becomes lighter in $200^O C$ H_2SO_4

experiments as the CrS/SO_4^{2-} ratio becomes greater than one before increasing again at the highest

CrS/SO_4^{2-} ratio. This is contrasted by the sulfate $\delta^{34}S$ trend that almost linearly increases with the

logarithmic increase in CrS/SO_4^{2-} ratio in these experiments. $\Delta^{33}S$ fractionation of sulfate also shows a

near linear increase in magnitude with increasing CrS/SO_4^{2-} ratio except with G-ASA-200 experiments,

which have almost no fractionation.

Unlike the H_2S_{Bulk} and residual sulfate relationship, the $\delta^{34}S$ trend of sulfate and CrS do not mirror

each other in anyway. $\Delta^{34}S_{CrS-Sulfate}$ displays an overall increase in magnitude from -9.82 to -13.36‰ with

increasing CrS/SO_4^{2-} ratio. However the highest fractionation factor is observed at moderate relative CrS

abundance in the G-ASA-200 experiments, which interestingly are the only runs that did not produce H_2S.

Also positive $\Delta^{34}S_{CrS-Sulfate}$ fractionations are observed in M-ASA-250 experiments which have

intermediate amounts of CrS. Unlike sodium sulfate experiments that have positive fractionation factors

between sulfate and reduced sulfur, the sulfate in these experiments are substantially fractionated. Like

the H_2S_{Bulk} and residual sulfate comparison experiments with CrS to sulfate rations less than one have

more fractionated CrS however when CrS/SO_4^{2-} ratios are greater than 1 higher magnitudes of CrS
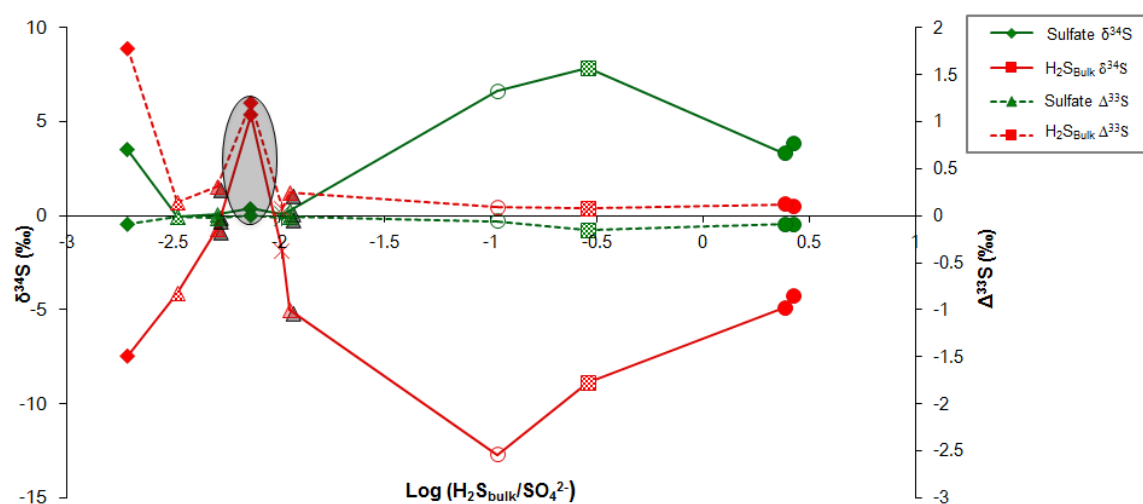
fractionation to sulfate fractionation are also observed.
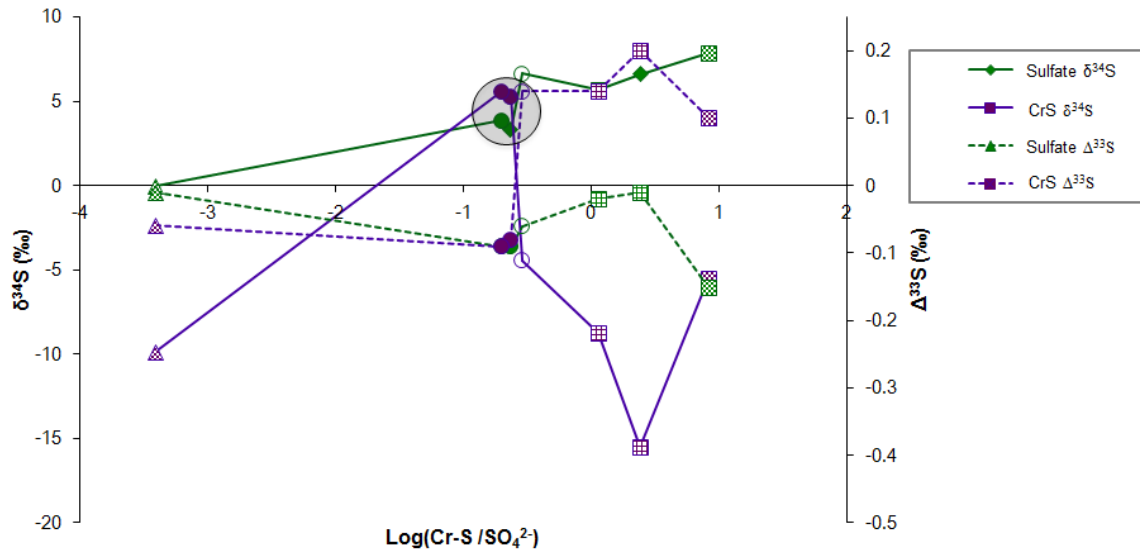
Figure 6: Relative CrS to Sulfate fractionation Comparison

$\delta^{34}S$ *of sulfate, solid green line, and CrS, solid purple line as a function of final the ratio of CrS to sulfate at the end of individual experiments plotted on the left axis.* $\Delta^{33}S$ *of sulfate, dotted green line, and CrS, dotted purple line, are plotted on the right axis.* $\Delta^{34}S$ *and* $\Delta^{33}S$ *fractionations between species for each experiment can be inferred from the relative difference on the left and right axis for solid and dotted lines respectively. The black shaded oval indicates the experiment where CrS is heavier that sulfate. Symbols for experiments are the same as those indicated for figures 2 and 3.*

3.2.4.3 Cr-S to H₂S relationship

$^{34}S/^{32}S$ fractionations between CrS and the final H$_2$S collections are summarized in table 3 and plotted against temperature in figure 7a. In every experiment H$_2$S is lighter than the polysulfide collected by chromium extraction providing $\Delta^{34}S_{H2SF-CrS}$ range between -15.46 and -0.34‰. In each experimental series the fractionation between these two species decreases with temperature. For mixture amino acid experiments the fractionation measured in the 200°C experiment is -8.29‰ and the maximum fractionation at 250°C is -4.08‰ showing a decrease of .84‰/10°C. The fractionation for glycine experiments decreases drastically in series run below 160°C, maximum $\Delta^{34}S_{CrS-H2SF}$ = -15.46‰, to series run at 170°C, maximum $\Delta^{34}S_{CrS-H2SF}$ = -7.05‰. From 170 to 258°C both G-SSA and G-ASA experiments together show a much less drastic linear decrease in fractionation with temperature of .43‰‰/10°C and .38‰/10°C respectively.

The magnitude of the $\Delta^{33}S$ difference between CrS and final measured H$_2$S shows the opposite trend with temperature that is observed in mass dependent fractionation. Figure 7b. shows that as temperature in G-SSA experiments increases the $\Delta^{33}S$ of H$_2$S$_{Final}$ becomes smaller than the $\Delta^{33}S$ of CrS. This trend is not linear as the difference in fractionation observed between 258 and 298°C is much greater than the change in fractionation over intervals at lower temperatures. Other experiments run with H$_2$SO$_4$ at 200°C and above also show small but significant depletions of relative ^{33}S in H$_2$S relative to CrS. For M-ASA experiments this difference increases from .06 to .14 per mil from 200 to 250°C. However despite these relative depletions in ^{33}S the $\Delta^{33}S$ of H$_2$S from TSR is still largely positive.
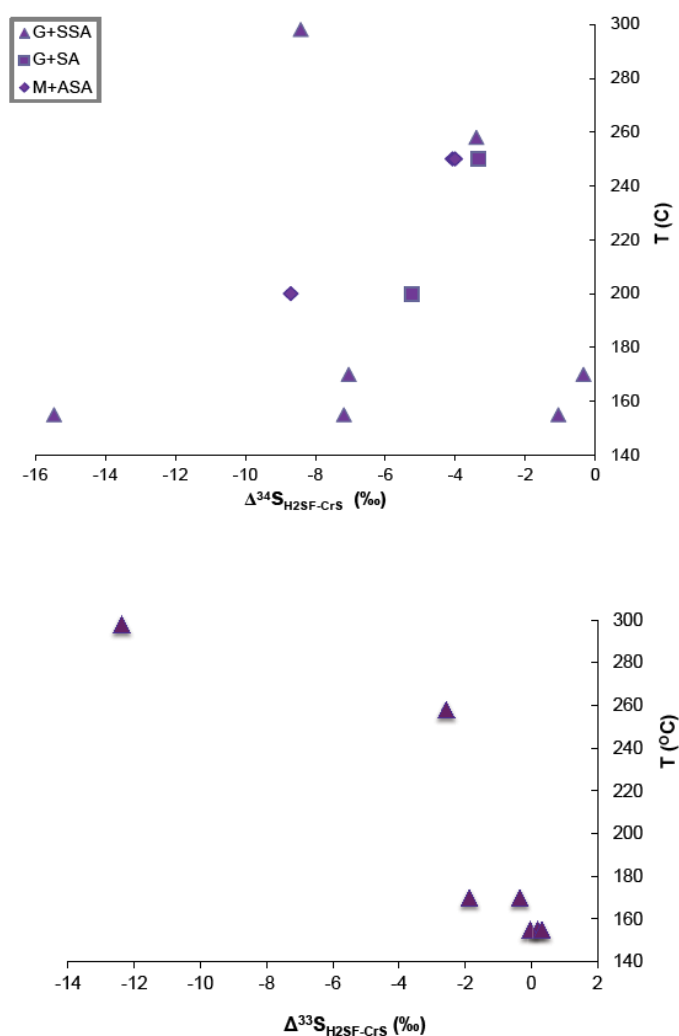
Figure 7:H₂S_F-CrS Fractionation with Temperature

Measured mass dependent (7a.) and mass independent (7b.) fractionation between H₂S and CrS collected at the end of experiments plotted against experimental temperature. Plot 7a.shows decreasing fractionation magnitude with temperature for mixture amino acid and anhydrous sulfuric acid (M-ASA) and glycine and sulfuric acid (G-SA) experiments between 200ᴼC and 250ᴼC. Glycine and sodium sulfate experiments (G-SSA) show a decrease in maximum fractionation of a given temperature range between 150ᴼC and 258ᴼC. Plot 7b shows increasing mass independent fractionation with temperature for glycine and sodium sulfate experiments.

3.2.4.4 Native sulfur and HCl-S isotope relation to H_2S

The $\delta^{34}S$ relationships between native sulfur collected over the course of H_2SO_4 experiments and bulk H_2S, and HClS and H_2S collected at the end of experiments is summarized in Table 3 and figure 8. In both relationships H_2S is depleted in ^{34}S with $\Delta^{34}S_{H2SF-HCl}$ relationships exceeding the $\Delta^{34}S_{H2SB-S0}$ values in each experiment. Both fractionations are greater in the M-ASA-200 experiment than either experiment at $250^O C$. The $\Delta^{34}S_{H2SF-HCl}$ increases by about 3‰ from -8.29 to -5.06‰ over this interval (.65‰/$10^O C$) while $\Delta^{34}S_{H2SB-S0}$ increases by roughly the same amount from -6.57 to -3.85‰. These temperature gradients are slightly less than those observed in $\Delta^{34}S_{CrS-H2SF}$ fractionations from the same experiments. $\Delta^{34}S_{H2SB-SO}$ from the glycine and H_2SO_4 run at $250^O C$ shows similar ^{34}S depletions in H_2S as the mixture amino acid experiment at $200^O C$ at -6.72‰.
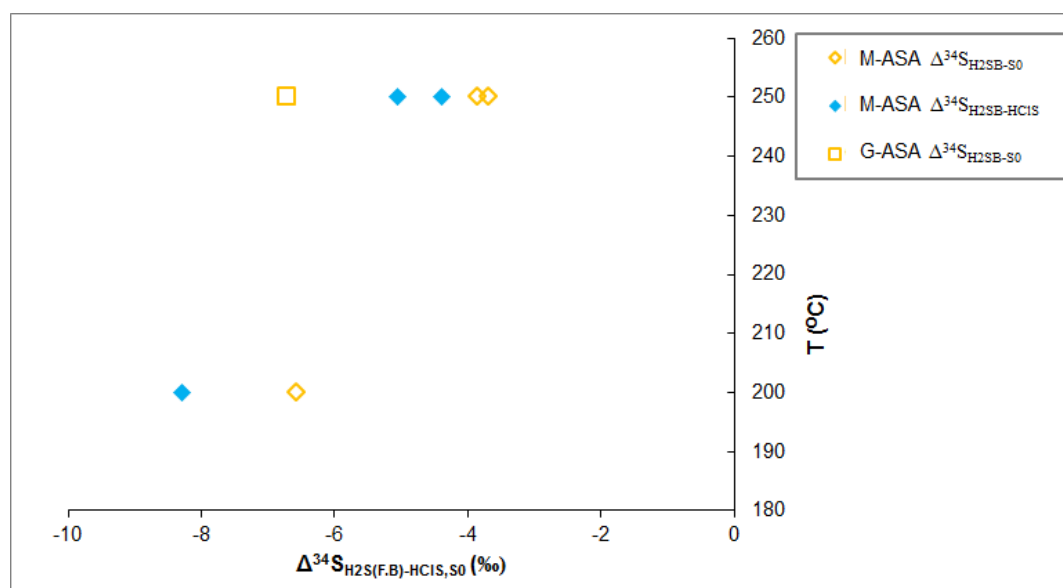
Figure 8: H₂S - Acid Extracted and Native Sulfur Fractionation with Temperature

3.2.5 $\Delta^{36}S$ and $\Delta^{33}S$ of TSR products

The $\Delta^{36}S$ and $\Delta^{33}S$ relationship of TSR products is summarized in figure 9. Reduced sulfur from TSR contains both positive and negative mass independent values in $\Delta^{36}S$ fractionation that covers a range from 1.39 to -1.26‰. Products of TSR contain both highly depleted and enriched relative amounts of ^{36}S to ^{33}S measured in $\Delta^{36}S/\Delta^{33}S$ fractionation ratios from +5 to -5. Small ^{36}S to ^{33}S fractionations are also observed in samples that have large mass independent $\Delta^{33}S$ values but $\Delta^{36}S/\Delta^{33}S$ ratios near zero. Glycine and sodium sulfate experiments produce both positive and negative mass independent $\Delta^{36}S$ values and only positive $\Delta^{33}S$ fractionations covering the right two quadrants of the $\Delta^{36}S/\Delta^{33}S$ Cartesian. The largest $\Delta^{36}S/\Delta^{33}S$ trends from these experiments are measured in H_2S while the magnitude of the $\Delta^{36}S/\Delta^{33}S$ ratio for CrS does not exceed .5. In G-SSA-258 and G-SSA-298, where complete ^{36}S analysis of H_2S and CrS was done, the $\Delta^{36}S/\Delta^{33}S$ slopes of total sulfide are in ranges of -5.5 to -.04 and -0.6 to -0.02 respectively. H_2S from M-SSA experiments all contain positive $\Delta^{33}S$ and positive $\Delta^{36}S$ values up to 1.39‰ covering the upper right quadrant of the $\Delta^{36}S/\Delta^{33}S$. These experiments show both high and low relative ^{36}S to ^{33}S fractionation with $\Delta^{36}S/\Delta^{33}S$ slopes between 1.35 and .21. However M-ASA experiments contain only negative $\Delta^{36}S$ values with maximum fractionations of -0.65‰. H_2S from these experiments containing positive and negative mass independent $\Delta^{33}S$ values were not measured however variations in the direction $\Delta^{33}S$ fractionation (enrichments and depletions of ^{33}S relative to ^{34}S) from measured samples all have the same $\Delta^{36}S$ direction (showing ^{36}S enrichment relative to ^{34}S) plotting in the lower two quadrants of the $\Delta^{36}S/\Delta^{33}S$ Cartesian. No sulfides plot in the upper left quadrant of mass independent depletion of ^{33}S and ^{36}S.
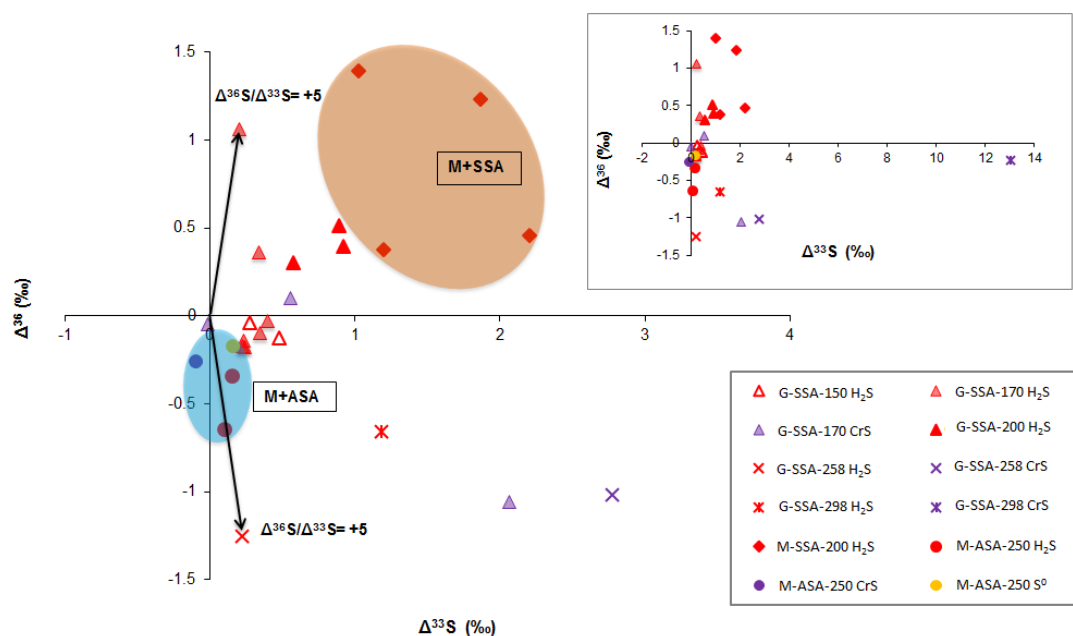
Figure 9: $\Delta^{36}S$ vs. $\Delta^{33}S$ Fractionation of TSR Sulfides

Mixture and sodium sulfate (M-SSA) and mixture and anhydrous sulfuric acid (M-ASA) data fall within the orange and blue shaded region respectively while wider ranges of $\Delta^{36}S$ and $\Delta^{33}S$ values are observed in glycine and sodium sulfate experiments. Maximum and minimum $\Delta^{36}S/\Delta^{33}S$ fractionation slopes, marked in black arrows, are observed in H_2S. The plot in the upper right has an extended x-axis is to include CrS with high mass independent fractionation of ^{33}S relative to ^{36}S.

4   Discussion

4.1 Experimental Conditions effect on Fractionation

4.1.1. Redox state of S: Sulfate vs. Sulfite

In comparing sodium sulfite and sodium sulfate experiments a decrease in formal oxidation state from +6 to +4 coincided with an increasing rate of H_2S production of about 4 orders of magnitude for experiments using glycine at $150^O C$. The experiments with the more reduced sulfur source also showed a smaller degree of maximum mass dependent fractionation ($\delta^{34}S_{Max}$= -20.82 and -4.67‰ for sodium sulfate and sodium sulfite respectively). This correlation between rate and isotope fractionation between sulfite and sulfate is indicative of the large energy barrier overcome in the reduction of the higher oxidation states of sulfur (Goldstein and Aizenshtat, 1994)**.** However $\delta^{34}S$ maximum of G-SSA-150 experiments occurs at one of the slowest measured rates of sulfate reduction and with in the data sets of both experimental conditions $\delta^{34}S$ values do not trend with rate. This implies that normal rate controlled kinetic isotope behavior cannot explain the ranges in mass dependent fractionation in individual series however it may explain the difference in the $\delta^{34}S_{Min}$ in sulfite and sulfate experiments.

Similar to $\delta^{34}S$ fractionation, $\Delta^{33}S$ fractionation is higher in sulfate experiments. This data show no overlap in range (.556-.18‰ and .04 to -.08‰ for sulfate and sulfite respectively). However the variation in $\Delta^{33}S$ of sulfate experiments shows no correlation to rate. This suggests that reduction of high oxidation states of sulfur cause higher degree of mass independent fractionation which is not necessarily controlled by kinetics. This also implies that the processes responsible for MIF-S signatures occur in early stages of TSR during the reduction of higher oxidation states of sulfur.
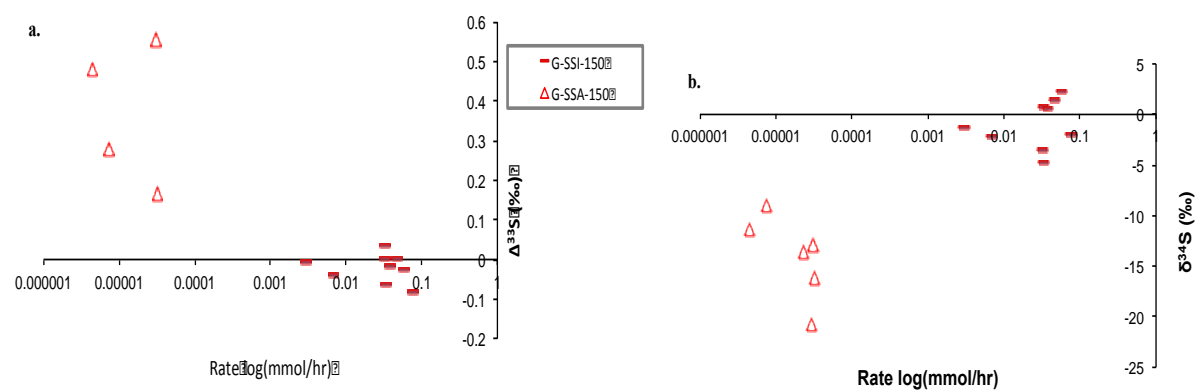
Figure 10: Sulfur redox state vs. rate comparison

Isotope data of glycine experiments run at 150-160°C are with sodium sulfate and sodium sulfite (G-SSA-150 and G-SSI) are plot against rate in δ^{34}S (a.) and Δ^{33}S (b.) measurements.

4.1.2. Temperature effects on fractionation

Temperature appears to have some effect on the H_2S production rates of sodium sulfate and glycine experiments between the ranges of 150 and $200^{O}C$. However the rate ranges were very similar for 170 and $200^{O}C$ experiments. The highest value was observed in the $200^{O}C$ series at .103 mmol/hr while reduction rates of $170^{O}C$ series reached a measured maximum of .07687 mmol/hr. The maximum rate of $150^{o}C$ experiments ($3x10^{-5}$) was still slower than the minimum rates of both 170 and $200^{O}C$ experiments which were $5x10^{-5}$ and $7x10^{-5}$ mmol/hr respectively.

The temperature effect on rate is more pronounced with the mixture amino acid and anhydrous H_2SO_4 experiments. At $250^{o}C$ H_2S production rates were up to two orders of magnitude greater than experiments run with same reactants at $200^{o}C$. They were also as slow as one order of magnitude slower when H_2S was collected at the end of experiments (range of $8.4x10^{-1}$ to $3x10^{-4}$ mmol/hr for $250^{o}C$ and 3.3 to $2.4x10^{-3}$ mmol/hr for $200^{o}C$).

In both the glycin-sodium sulfate and mixture-sulfuric acid comparisons $\delta^{34}S_{Min}$ (-20.82 and -13.14‰ respectively) occurs at the lower temperatures and at comparatively slower rates. However M-ASA-250 experiments have vastly different mass dependent fractionations than H_2S produced from M-ASA-200 experiments at the same rate. Increasing $\delta^{34}S$ values measured in time and lower production rates in $250^{O}C$ experiments may be indicative of Rayleigh distillation however fractionation from initial sulfate (0‰) is much greater early in the experiments when rates are above $1x10^{-1}$ mmol/hr (up to -9.90‰) than from the final sulfate and H_2S collected at the end of experiments where production rates were below $1x10^{-2}$ (up to -2.30‰) (refer supplemental table for complete experimental isotope data) indicating changes in fractionation magnitude that cannot be explained through simple distillation. The comparatively large degree of fractionation for the high fractions of H_2S measured early in $250^{0}C$ experiments may also indicate fractionation factors that are greater than those observed in H_2S from $200^{o}C$ experiments. Here the relative starting sulfur recovered as H_2S in the initial collection was nearly

3 times greater than that at 200°C (3.70 to 1.36%) but achieved ¾ the δ^{34}S fractionation (-9.9 to -12.14‰).

For glycine and sodium sulfate experiments above 160°C temperature and rate appear to have little effect of δ^{34}S fractionation. From a rate range of 4.4×10^{-4} to 1.03×10^{-1} mmol/hr the minimum δ^{34}S values fluctuate less than 1.5‰ (from -5.19 to -6.5‰). Furthermore positive δ^{34}S values up to 4.98‰ are observed at relatively slow production rates at 170°C. This trend does not correlate with time and total reduced sulfur is too low in these experiments for this to be explained by Rayleigh distillation. This observation shows a lack of correlation between rate and fractionation in this temperature range.

The effect of temperature on Δ^{33}S fractionation is quite obvious in both comparisons. Despite any overlap in rate the G-SSA-200 and M-ASA-250 experiments show the highest fractionations relative experiments run at lower temperatures under similar conditions. The maximum values for glycine-sodium sulfate experiments at 200°C, above .85‰, are achieved at relatively high rates of H_2S production, above 1.0×10^{-2} mmol/hr, while fractionations from 170°C experiments at this rate range reach a maximum of .18 ‰. At temperatures below 200°C higher maximum Δ^{33}S values are measured in G-SSA-150 experiments compared to G-SSA-170 experiments. However there is considerable overlap of Δ^{33}S fractionation in both experiments over a wide range of rates. A Δ^{33}S value of 1.17‰ in glycine-sodium sulfate experiments over 250°C further emphasizes the correlation between temperature and mass independent fractionation.

In the mixture-sulfuric acid experiments at 250°C Δ^{33}S values were twice as fractionated in the same direction as M-ASA-200 when rates were over two orders of magnitude greater. When the rate of 250°C experiments were an order of magnitude less than 200°C experiments the magnitude of Δ^{33}S fractionation was also twice as high but in the opposite direction. Like the trend in δ^{34}S, this change in fractionation direction does not appear to be due to Rayleigh distillation, in fact over the course of these experiments Δ^{33}S fractionation of H_2S goes from positive to negative with respect to sulfate. This may

indicate a fundamental change in the mechanism of fractionation which reverses the $\Delta^{33}S$ fractionation from sulfate.
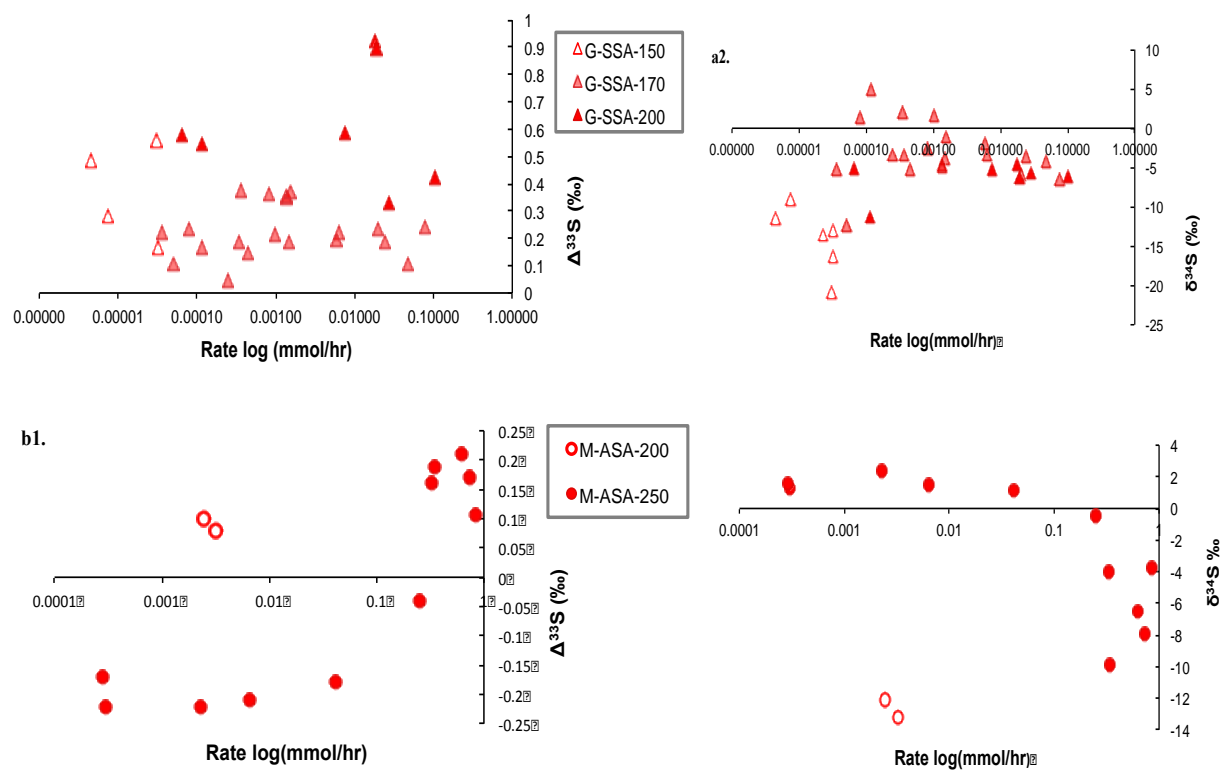
Figure 11: Temperature vs. Rate Comparison

Isotope data of H_2S from G-SSA Experiments run at $150\text{-}160^OC$, 170^OC, and 200^OC plotted against rate in $\delta^{34}S$ (a1.) and $\Delta^{33}S$ (a2.) measurements using empty, shaded, and solid triangles. Isotope data from H_2S of M-ASA experiments run at 200^OC (empty circles) and 250^OC (solid circles) plotted against rate in $\delta^{34}S$ (b1.) and $\Delta^{33}S$ (b2.) measurements.

4.1.3. Reductant effect on fractionation

Amino acid type used to reduce sulfur appears to have variable effects on H_2S production rates. Alanine and glycine experiments with sodium sulfate carried out in runs between 150 and 180°C have very similar maximum production rates on the order of $1x10^{-3}$ mmol/hr. However when alanine and glycine are reacted together in mixture amino acid experiments the maximum recorded production rate is lower than runs with just glycine with sodium sulfate at 200^{0}C by over an order of magnitude ($2.3x10^{-3}$ to $2.78x10^{-2}$ mmol/hr). This, along with isotope data discussed later, implies that at elevated temperatures glycine and alanine mixtures react in a unique manner that differs from the average of their individual results. Interestingly in experiments that reduce H_2SO_4 at 250°C mixtures of amino acids produce much more H_2S than glycine experiments. Both these series of experiments have comparable amounts of total reduced sulfur (32.83% and 36.13 to 40.94% for glycine and mixture experiments respectively) thus demonstrating the possible importance of reactions between amino acids in creating hydrogen (water) for H_2S production (Goldhaber and Orr, 1995).

For mixture-sodium sulfate experiments at 200°C $\delta^{34}S$ values in the positive and negative direction appear unaffected by rate as a reduction rate of $1.4x10^{-3}$ mmol/hr produced a sample with a $\delta^{34}S$ of -7.33‰ and a H_2S production rate of $2.4x10^{-3}$ mmol/hr had a value of +15.50‰. Furthermore that latter sample was measured in the first H_2S collection of that experiment demonstrating the random $\delta^{34}S$ fractionations of some experiments. G-SSA-200 shows a consistent range of $\delta^{34}S$ values between -6.22 and -4.63‰ over a large range of H_2S production rates with the lone deviation in negative fractionation (-11.34‰) coming at one of the lowest measured production rates. The comparison between these two series demonstrates the importance type of organic reductant, as opposed to kinetics, in creating the variation and trends of $\delta^{34}S$ fractionation.

The comparison between glycine and alanine in sodium sulfate experiments at 150 to 180°C shows that they produce H_2S with similar $\delta^{34}S$ values under the same rates. Alanine however produces some heavier fractionation at higher rates while slower rates observed in glycine experiments produce

lighter values. The similarity in $\delta^{34}S$ values over the observed rates shows that the differences in fractionation based on these amino acids types is minimal especially in reference to the comparison between glycine and mixture amino acid experiments at $200^{\circ}C$.

M-ASA-250 experiments are also able to produce vastly different $\delta^{34}S$ to rate relations than those observed in G-ASA-250 experiments. H_2S produced at nearly three orders of magnitude faster in mixture amino acid experiments had a higher degree of mass dependent fractionation than glycine experiments (-9.9 to 8.95‰ respectively) this once again shows of mixtures of amino acids have vastly different fractionation effects.

Mixture amino acid experiments also show distinguishably higher degrees of mass independent fractionation regardless of rate in comparison to glycine in sodium sulfate and H_2SO_4 experiments. Between the comparatively narrow range of H_2S production rates for M-SSA-200 experiments ($4.0x10^{-4}$ and $3.4x10^{-3}$) $\Delta^{33}S$ values are over twice as fractionated as values measured in glycine over rates of $7x10^{-5}$ to $1.0x10^{-1}$ mmol/hr. The mixture amino acid experiments produce $\Delta^{33}S$ values between 2.20 and .48 per mil over this rate range implying that mass independent fractionation for these experiments is not related to normal kinetic behavior. Glycine experiments actually show their highest degree of mass independent fractionation near the faster end of their rate range ($\Delta^{33}S= .93$‰ at $1.8x10^{-2}$ mmol/hr) once again displaying lack of kinetic relationship in mass independent fractionation. This is opposite the rate relation for $\delta^{34}S$ in glycine where more fractionated samples were produced at lower rates showing how mass independent and mass dependent are fractionated differently by the same conditions.

In M-ASA-250 experiments both fast and slow production rates ($6.3x10^{-1}$ to $3x10^{-4}$ mmol/hr) created H_2S with mass independent signatures while at slow rates ($4x10^{-4}$ mmol/hr) glycine did not. The $\Delta^{33}S$ relationship between glycine and alanine at $150-180^{\circ}C$ with sodium sulfate, however, is similar the one observed in $\delta^{34}S$ fractionation; a similar range of values of mostly mass dependent fractionation with slightly higher, mass independent, fractionation from the experiment with glycine ($\Delta^{33}S = .22$‰) at slower rates and values closer to zero for experiments with alanine at faster rates.
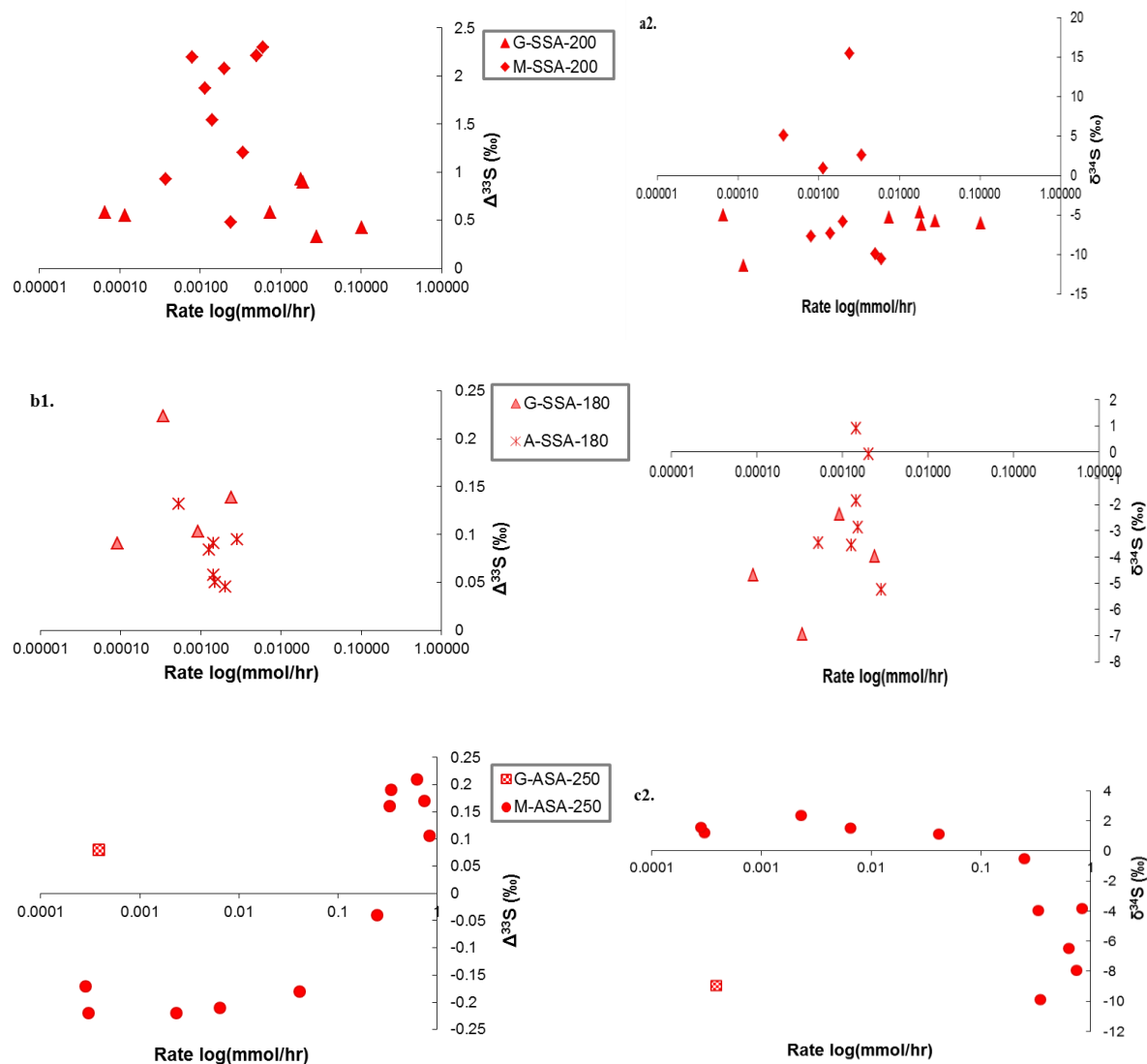
Figure 12: Reductant vs. Rate Comparison

Isotope data of H₂S from G-SSA-200 (Triangles) M-SSA-200 (Diamonds) plotted against rate in $\delta^{34}S$ (a1.)

and $\Delta^{33}S$ (a2.) measurements. Isotope data of H₂S from G-SSA-180 (Shaded triangles) and A-SSA-180

(star) plotted against rate in $\delta^{34}S$ (b1.) and $\Delta^{33}S$ (b2.) measurements. Isotope dataG-ASA-250 (patched

squares) and M-ASA-250 (solid circles) plotted against rate in $\delta^{34}S$ (C1.) and $\Delta^{33}S$ (C2.) measurements.

4.1.4. Effect of Sulfate Type

Experiments that reduce H_2SO_4 produce H_2S at higher rates than those with sodium sulfate. This is consistent with results that suggest lower pH levels decrease the activation energy for TSR (Anisimov 1978). In glycine experiments at 200^0C the maximum rate was 5.5×10^{-1} mmol/hr and 1.0×10^{-1} for dissolved H_2SO_4 and sodium sulfate runs respectively. For mixture amino acid experiments at 200^OC the maximum production rates for undissolved H_2SO_4 and sodium sulfate experiments were quite similar, 2.4×10^{-3} and 3.4×10^{-3} mmol/hr, however H_2S was likely limited with no additional water in the H_2SO_4 experiments despite much having high amounts of total sulfur reduced and thus higher rates of reduction. In M-ASA-250 experiments, a larger amount of total reduced sulfur is collected as H_2S and reduction rates are over two orders of magnitude greater than the M-SSA-200 experiments.

Despite the rate effects of sulfur type, the $\delta^{34}S$ fractionation is similar for both sodium sulfate and H_2SO_4 glycine experiments. At faster rates above 1.0×10^{-2} mmol the $\delta^{34}S$ range for G-SSA-200 experiments is -4.63 to -6.22‰ and -3.01 to -6.50‰ for H_2SO_4 experiments. At rates below 1.0×10^{-3} mmol/hr the $\delta^{34}S$ fractionation reaches -9.73 and -11.37‰ for H_2SO_4 and sodium sulfate experiments respectively. For mixture amino experiments at 200^OC samples produced from H_2SO_4 are light, $\delta^{34}S_{Min}$ of -13.14‰, compared to those from sodium sulfate produced at similar or slower rates, $\delta^{34}S_{Min}$ of -7.69‰. In fact H_2S produced at much higher rates in M-ASA-250 experiments are also more negatively fractionated than sodium sulfate experiments that also contain mixtures of amino acids. This increase in mass dependent fractionation is opposite that expected for the presumed lower activation energy reactions of these experiments.

The effect of sulfur type on $\Delta^{33}S$ fractionation is easily described in both comparisons. In glycine and mixture series the maximum $\Delta^{33}S$ fractionation of H_2SO_4 experiments was less than the minimum $\Delta^{33}S$ values of the sodium sulfate experiments. In fact for samples of similar production rate fractionation was about an order of magnitude greater for sodium sulfate experiments in both series. After accounting

for rate, this comparison suggest that a highly acidic sulfur source reduces the mass independent

signatures of TSR however it does not reduce the amount of mass dependent fractionation. In mixture

amino acid series, where mass independent fractionation was comparatively higher than glycine runs, the

acidic sulfur experiments actually produced lighter fractionation along with smaller mass independent

signatures in H_2S. Discussion of a mechanism that increases $\Delta^{33}S$ and $\delta^{34}S$ values will be discussed in

section 4.2.2.2.
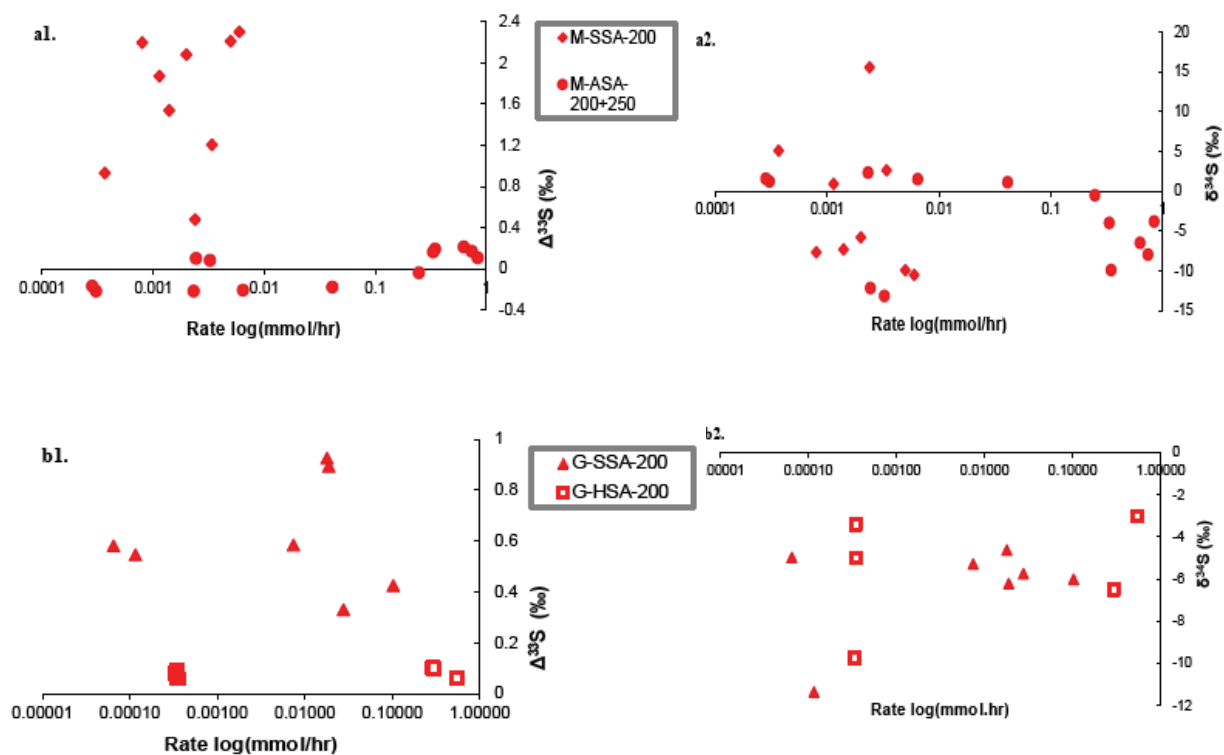
Figure 13: Sulfate Characteristics vs. Rate Comparison

Isotope data of H₂S from M-SSA-200 (diamonds) and M-ASA-200+250 (circles) plotted against rate in δ³⁴S (a1.) and Δ³³S (a2.) measurements. Isotope data of H₂S from G-SSA-200 (triangles) and G-HSA-200 (star) plotted against rate in δ³⁴S (b1.) and Δ³³S (b2.) measurements.

Comparison	Rate	$\delta^{34}S_{Min}$	With R	$\delta^{34}S_{Range}$	With R	$\Delta^{33}S$	With R
SO_4^{2-} to SO_3^{2-}	↑	↑	YES	↓	YES	↓	YES
Low T to High T	↑	↑	YES	↑	NO	↑	NO
Glycine to Alanine	↑	↑	YES	same	NO	↓	YES
Glycine to Mix	same	same	NO	↑	NO	↑	NO
Na_2SO_4 to H_2SO_4-Mix	↑	same	NO	↓	NO	↓	NO
Na_2SO_4 to H_2SO_4-Glycine	↑	↑	YES	same	YES	↓	NO

Table 4: Experimental condition comparison summary

Six key comparison's general effects on rate of H_2S production, the minimum $\delta^{34}S$ value, the $\delta^{34}S$ range, and magnitude of $\Delta^{33}S$ fractionation from the previous discussion are summarized. Up arrows indicate an increase in value from one condition to the other labeled in the comparison while down arrows indicate decreases in values. For isotope effects YES or NO indicate if these changes show some sort of rate dependence. Isotope effects described in red indicate interesting fractionation behavior that may be explained by VEDE in the following discussion.

4.2 Mechanisms of Isotope fractionation

4.2.1. The kinetic isotope effect

Thus far discussion has focused on the complexities of fractionation during TSR. It is therefore difficult to describe the results with one method (mechanism) of fractionation. The discrepancies between trends of in $\delta^{34}S$, $\Delta^{33}S$, and $\Delta^{36}S$ fractionation suggest that mechanisms responsible for large $\delta^{34}S$ fractionations may not be the cause of large mass independent variations. Our analysis has allowed us to evaluate the presence of kinetic isotope effects during TSR by comparison of rate, temperature, and experimental product abundance. In ^{34}S fractionation several observations may be explained by kinetic isotope effects. These are most strongly observed in the mass dependent relationship of different sulfide species the same experiment. As stated in sections 3.2.4.3 and 3.2.4.3 gaseous fully reduced sulfur collected as H_2S is lighter than other TSR products. Based on the total energy required for the large redox transition from initial sulfate and conversion from the solid-liquid system to H_2S gas it is suggested that sulfur in H_2S has experienced the highest amount of chemical (energetic) processes (Goldhaber and Orr 1995). This has inflicted large kinetic effects reflected in its low $\delta^{34}S$ values relative to other sulfur species. This is further supported by the dependence of fractionation on temperature where experiments with more energy inputs in heat had relatively higher amount of ^{34}S overcome the activation barriers to the end TSR product. Although variability and magnitude of $\delta^{34}S$ ranges is substantial in the H_2S produced by TSR kinetic isotope effects may explain the maximum ^{34}S depletion ($\delta^{34}S_{Min}$) in products of some series relative to others. Such observations found in sulfate relative to sulfite at 150 to $160^{O}C$ and G-SSA-150 experiments relative to ones at higher temperature are consistent with the lower rates of H_2S production and may be explained by kinetic isotope effects.

This is further reflected in the fractionation of the residual sulfate pool collected at the end of experiments. In almost all experiments the bulk reduced sulfur and sulfate are fractionated in the opposite direction with sulfate becoming heavier than its initial value and containing small but negative $\Delta^{33}S$ values compared to the positive values observed in sulfide. Although the scaling of fractionation between

sulfate and sulfide varies, (figures 5 and 6) by scaling sulfate fractions to amount CrS produced at the end

of experiments some degree of Rayleigh or distillation behavior is observed in in the δ^{34}S and Δ^{33}S trends

of sulfate.

4.2.2. Characteristics of mass independent fractionation during TSR

The mass independent behavior of TSR products creates large Δ^{33}S values and ranges, large range

in λ values, large Δ^{33}S values, and large ranges in Δ^{36}S/Δ^{33}S ratios. Our data clearly demonstrates that no

fractionation trend may explain the isotope ratios in the products of TSR and that λ values may be

observed above and below mass dependent fractionation slopes. Experiments that produce mass

independent fractionation measured in Δ^{33}S values such as mixture amino acid and sodium sulfate runs

and high temperature glycine and sodium sulfate experiments produced large ranges in λ values. Our data

also shows that λ values can not used to predict the degree of mass independent fractionation measured in

Δ^{33}S values as seen in the large range of Δ^{33}S values that have a common λ on figure 2a.   However

positive and negative trends in $\Delta^{33}S_{H2S-H2S}/\Delta^{34}S_{H2S-H2S}$ are observed. Despite these trends almost all MIF-S

signature in TSR sample are due to relative ^{33}S enrichment with respect to ^{34}S regardless if samples have

higher ^{34}S/^{32}S ratios than starting or residual sulfate. MIF-S samples with negative Δ^{33}S values thus far

have only been observed after large amounts sulfur reduction in high temperature experiments suggesting

the only systematic change in mass independent isotope fractionation that may be understood with out

invoking the conditions that effect Δ^{33}S magnitude as described in section 4.1.2 and 4.1.3. Overall Δ^{33}S

values are harder to characterize than mass dependent fractionation through rate (kinetic) correlation

suggesting processes responsible for creating MIF-S signatures are not due to normal kinetic isotope

effects. TSR showed random variations of fractionation factors between the residual sulfate and sulfide

measured in H_2S_{Bulk} or CrS and lack of identifiable trends in fractionation with relative abundance, and

lack of δ^{34}S and Δ^{33}S fractionation correlation. This variation in relative fractionation suggest more than

one mechanism is fractionating the $\delta^{34}S$ and $\Delta^{33}S$ value of sulfide either during or after they acquire MIF-S signatures.

4.2.3. Magnetic isotope Effects During TSR

The influence of spin selective processes responsible for the magnetic isotope effects is observed in the isotopic relationship between CrS and H_2S. CrS is enriched in ^{33}S relative to H_2S when $\Delta^{33}S$ fractionation is large. This fractionation increases at high temperatures. However the mass dependent relationship with temperature shows normal kinetic behavior where fractionation between CrS and H_2S is higher at lower temperatures. To produce sulfide with positive $\Delta^{33}S$ values mass dependently a kinetic fractionation slope would need to be less than .515. This has been observed in bacterial sulfate reduction experiments (Johnston et. al., 2005). Therefore higher $\Delta^{33}S$ values may be explained by larger kinetic influences. This is the opposite of the relationship observed between CrS and H_2S where larger kinetic fractionations correlate with smaller $\Delta^{33}S$ fractionation. Therefore another mechanism is responsible for the $\Delta^{33}S$ fractionation which enriches CrS in ^{33}S relative to H_2S. We suggest the creation spin selective organic radicle intermediate enriched in ^{33}S like that described by Oduro et. al. (2011) that forms at high temperatures. During the reduction processes this may form a significant fraction of the CrS collected at the end of experiments if other polysulfides are further reduced through non spin selective steps to H_2S. The formation of this radical thus leaves a ^{33}S depleted sulfide pool with smaller $\Delta^{33}S$ values that may form H_2S by the kinetic isotope effect thus creating the mass dependent trend with temperature as previously described. The isotopic composition of CrS is thus a function of how much radical is formed and how much H_2S gets reduced from the residual, non spin selective and ^{33}S depleted, polysulfide and organic sulfur species formed before the radical. At high temperatures both these factors are large leading to a higher ratio of CrS radical to other CrS species which is manifested in larger $\Delta^{33}S$ differences between chrome extractable sulfur and H_2S.

This schematic is summarized in figure 14c. and 14d. At high temperatures the formation of CrS proceeds with little fractionation along the hypothetical kinetic fractionation slope. However the creation of a CrS spin selective radicle causes large Δ^{33}S fractionation without affecting ratios of even number nuclei then ^{34}S depleted H_2S is formed from the remaining CrS. At lower temperatures larger fractionations are observed during reduction and creation of H_2S along the kinetic fractionation line leading to lighter δ^{34}S values than those that arise from high temperature experiments. The low abundance of spin selective radicals and higher amount of other organic sulfide that doesn't get fully reduced leads to less mass independent fractionation observed between CrS and H_2S. This fractionation mechanism is further supported by the Δ^{36}S/Δ^{33}S ratios of CrS all of which are between -1 and 1. This means they exhibit higher amounts of mass independent fractionation on the odd number nuclei than the even number nuclei which is consistent with contribution from ^{33}S spin selective radical. Likewise H_2S with positive Δ^{33}S values but higher relative Δ^{36}S fractionation is consistent with their formation from sulfur depleted in ^{33}S.

4.2.4. VEDE during TSR

While the magnetic isotope effect can explain the relationship between CrS and H_2S it cannot explain the overall mass independent fractionation characteristics of TSR products. Specifically H_2S from TSR that are mass independently fractionated contain almost exclusively positive Δ^{33}S values, especially ones with small δ^{34}S fractionation, which cannot be reconciled by the MIE. Nor can it explain experiments that produce bulk sulfur and CrS that are heavier than residual sulfate. Also, as noted on figure 14c. and 14d., if the magnetic isotope effect was the sole source of MIF-S signatures we would expect to see negative Δ^{33}S$_{H2S-H2S}$/Δ^{34}S$_{H2S-H2S}$ trends with temperature but in fact we see the opposite in G-SSA experiments. Lastly we would not expect any positive Δ^{36}S values H_2S produced from TSR but experiments with mixture amino acids and glycine all contain positive MIF-S Δ^{36}S values.   However all

these discrepancies may be explained by the VEDE effect. Further discussion will describe how the VEDE manifest itself during TSR.

Perhaps the most supportive evidence for sulfur fractioned by VEDE is the correlation between positive $\Delta^{33}S$ values and temperature in H_2S. This is predicted for reactions where there is a lower number of bound states for ^{32}S relative to all other isotopes. Higher temperatures puts more reactants at the highest energy levels thus increasing the number of bond discontinuities between ^{32}S and all other sulfur isotope molecules This reaction must happen before the fractionation of Cr-S to create positive $\Delta^{33}S$ values in H_2S relative to starting sulfur but negative $\Delta^{33}S$ values relative to CrS. Negative $\Delta^{33}S$ values of residual sulfate are thus created by fractionations of discontinuities in the unbound sulfur of this reaction.

Variables such as reductant type that effect $\delta^{34}S$ and $\Delta^{33}S$ fractionation despite no kinetic justification may be due to how they affect the subtle energetics of reactions responsible for vibrational isotopologue discontinuities. This may explain the increased $\delta^{34}S$ and $\Delta^{33}S$ fractionations resulting from experiments with mixtures amino acids. This cannot be predicted by the combined fractionation effects glycine and alanine or reconciled through or changes rate of sulfide production. Instead VEDE suggest combinations of different organic types have a unique potential to create MIF-S signatures due to how they interact with sulfate.

Similarities in the $\delta^{34}S$ range and minima between H_2SO_4 and Na_2SO_4 (section 4.1.4) experiments despite the reduced reduction rates observed in the latter may also be explained if the mass independent signatures in these experiments were acquired by VEDE. Increased VEDE in Na_2SO_4 experiments would inflict larger positive $\delta^{34}S$ fractionation on reacted sulfur. Therefore even if the mass dependent ^{34}S depletions from kinetic isotope effects during reduction are greater in these experiments the differences in H_2S would be offset by the positive $\delta^{34}S$ fractionation from the VEDE. Mass dependent overlap observed between high MIF-S samples from high temperature more energetically favorable experiments, such as G-SSA-200, and lower temperature experiments, G-SSA-170, which produced low MIF-S samples is

reconciled by the VEDE. Since increased temperature is predicted to decrease positive $\delta^{34}S$ fractionation for sulfur cluster experiencing VEDE and decrease the negative $\delta^{34}S$ fractionation from the KIE sufficient overlap in the $\delta^{34}S$ values of H_2S may occur with low temperature reactions under otherwise the identical conditions where these opposing mass dependent fractionation effects are larger. The mass dependent fractionation from VEDE would also explain the positive $\delta^{34}S$ values measured CrS, early H_2S collections and H_2S_{Bulk} relative to residual sulfate. It also explains why $\delta^{34}S$ and $\Delta^{33}S$ values of products and residuals of experiments that experience little MIE do not scale since the KIE also contributes to mass dependent fractionation.

Lastly the $\Delta^{36}S$ range may only be explained by VEDE where variables affecting the energy of early TSR reactions create bond discontinuities between different S isotopologues. This can create varying contributions of positive and negative $\Delta^{36}S$ fractionation seen glycine experiments. This also explains mixed amino acid and sodium sulfate experiments that have distinctively positive $\Delta36S$ values and mixed amino acid-H_2SO_4 experiments which all have negative $\Delta^{36}S$. The change from positive to negative $\Delta^{33}S$ fractionation observed in the later stages of M-ASA-250 experiments may be due to drastic changes in the energetics of TSR over the course of a reaction which alter the dissociation energy thus causing a bond discontinuity jump from ^{32}S to ^{33}S. In glycine-sodium sulfate experiments above $250^{O}C$, where there is complete ^{36}S analysis of TSR products, the $\Delta^{36}S/\Delta^{33}S$ fall ratios with in ranges which would be expected for the ^{32}S VEDE discontinuity and are too shallow (too much $\Delta^{33}S$ fractionation) to be reconciled but kinetic isotope effects
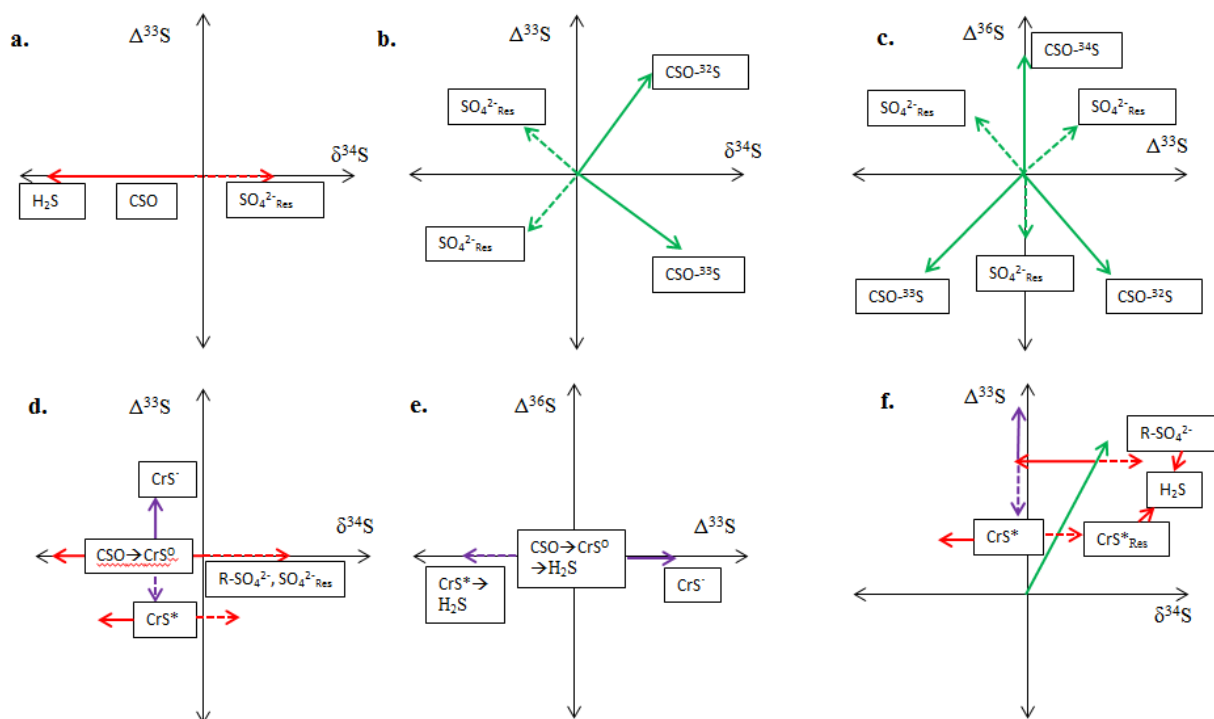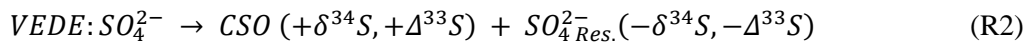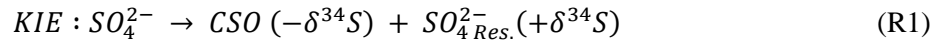
Figure 15: Isotope Schematic of individual TSR Steps

a. $\Delta^{33}S$ vs. $\delta^{34}S$ diagram of mass dependent fractionation through equation R1 in step 1 showing fractionation of residual sulfate containing positive $\delta^{34}S$ values with the dotted line and organically bound oxidized sulfur, CSO (and eventually H_2S,) containing negative $\delta^{34}S$ values with the solid line. **b.** $\Delta^{33}S$ vs. $\delta^{34}S$ diagram of fractionation caused by discontinuities in the bond state of ^{32}S and ^{33}S through equation R2 in step 1 leading to the formation of CSO compounds with positive $\delta^{34}S$ values and opposing $\Delta^{33}S$ (solid line) and residual sulfate (dotted line). Note that discontinuity of the ^{34}S bound state does not cause fractionation on this diagram. **c.** $\Delta^{36}S$ vs. $\Delta^{33}S$ diagram of R2. discontinuities in the bond state of ^{32}S and ^{33}S both create CSO compounds with negative $\Delta^{36}S$ values while ^{34}S discontinuities creates CSO compounds with positive $\Delta^{36}S$ values. **d.** $\Delta^{33}S$ vs. $\delta^{34}S$ diagram of showing the effects of the kinetic and magnetic isotope effects in R3 and R4 in step 2 with out any fractionation by the VEIDE in during step 1. Mass dependent fractionation through the KIE leads to the formation CrS^O from CSO and then at elevated temperatures the formation of $CrS^{\cdot}$ causes the residual sulfide, CSO*, with negative $\Delta^{33}S$ values. Note that the KIE is larger (length of the of the top red solid arrow) for low temperature reduction when the effects of the MIE are small. With out reaction R2 this would cause H_2S to have almost exlusively negative $\delta^{34}S$ and $\Delta^{33}S$ values and a negative $\Delta^{33}S_{H2S-H2S}/\Delta^{34}S_{H2S-H2S}$ fractionation with temperature, which is not observed in experiments. **e.** $\Delta^{36}S$ vs. $\Delta^{33}S$ diagram of the MIE in R4 which results in $CrS^{\cdot}$ with positive $\Delta^{36}S$ values. Note that with out reaction R2 this would result in no positive $\Delta^{36}S$ fractionation. **f.** $\Delta^{33}S$ vs. $\delta^{34}S$ diagram of reaction R6 involving oxidized sulfur compunds from the residual of R3 and sulfide compounds from the residuals of R4 and R5 that are not reduced to H_2S. As shown this results in H_2S with positive δ^{34} values and smaller $\Delta^{33}S$ values than those resulting from R2 (green line).

5   Synthesis of fractionation steps during TSR

Based on the fractionation of different sulfur species and the identification of the different mechanism responsible during those fractionations we can develop a sequence composed of three major steps responsible for the isotope values observed during TSR. The first step is the interactions between sulfate and the amino acid which are responsible for the isotopic signature of sulfate and the initial fractionations of sulfides collected during and at the conclusion of experiments. The second step is the creation of organically associated polysulfides through reduction of sulfate. The third step is the further reduction of some of these sulfide species and creation of H_2S. The relative magnitude of fractionation related to temperature as well as amino acid type during these steps may also be inferred based on the mechanism. A schematic for this mechanism influence by these conditions in the $\Delta^{33}S$ vs. $\delta^{34}S$ and $\Delta^{36}S$ vs. $\Delta^{33}S$ Cartesian is summarized figure 15. The following reactions and accompanying diagrams in figure 14 describe fractionations associated with each step.

Step 1:

$$KIE : SO_4^{2-} \rightarrow CSO\ (-\delta^{34}S) + SO_{4\,Res.}^{2-}(+\delta^{34}S) \tag{R1}$$

$$VEDE: SO_4^{2-} \rightarrow CSO\ (+\delta^{34}S, +\Delta^{33}S) + SO_{4\,Res.}^{2-}(-\delta^{34}S, -\Delta^{33}S) \tag{R2}$$

The cumulative kinetic isotope effect in all three steps drives the products of TSR to be depleted in ^{34}S relative to starting sulfur making the residual sulfate heavier as noted in previous TSR experiments (Goldstein and Aizenshtat, 1994). This effect is largely responsible for the positive $\delta^{34}S$ values observed in TSR residual sulfate especially those from experiments with high-reduced sulfur yields. H_2S may be produced from the kinetic isotope effect with out any mass independent fractionation from the other two mechanisms if the reductant permits no spin selective intermediaries to be created

during the reduction processes and if there are no VEDE. The pathway is noted with the box labeled

"R1" along the X axis of figure 15a. It is likely that most sulfur gets reduces through this pathway during

TSR based in mostly ^{34}S depleted products especially in low temperature experiments where fractionation

from the other described mechanisms is minimal.

Step one may also fractionate through vibrational energy discontinuity isotope effects

(schematically shown in figures 14b. and 14c. and labeled 'R2' on figure 15a. and 15b.). This creates

organically bound or initially reduced sulfur with positive δ^{34}S, positive Δ^{33}S, and negative Δ^{36}S values

through discontinuity of the in ^{32}S bond number labeled CSO in figure 14. The residual sulfate from

VEDE-32 is thus fractionated in the negative δ^{34}S and Δ^{33}S direction while incurring positive Δ^{36}S values.

At higher temperatures the mass dependent fractionation decreases while mass independent fractionation

increases for reacted and residual sulfur. This is schematically shown with the steeper green fractionation

trend line (larger λ) in figure 15a. The temperature effect on R2 thus creates lower δ^{34}S fractionations in

sulfides and higher δ^{34}S fractionations in sulfate with out and kinetic effects. In figure 15b the green

fractionations lines increase in length compared to those for low temperatures but maintains the same

Δ^{36}S/Δ^{33}S trend.

Step 2

$$KIE : CSO\ (+\delta^{34}S, +\Delta^{33}S)\ \rightarrow\ CRS^{O}\ (-\delta^{34}S) +\ SO_2, SO_3^{2-}, R-SO_4^{2-}\ (+\delta^{34}S)\ (R3)$$

$$MIE: CSO\ (+\delta^{34}S, +\Delta^{33}S)\ \rightarrow\ CRS^{O}\ (-\delta^{34}S)\ \rightarrow CrS^{*}\ (+\Delta^{33}S) + CrS'\ (-\Delta^{33}S)\ (R4)$$
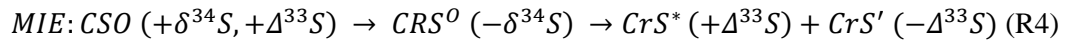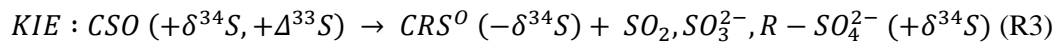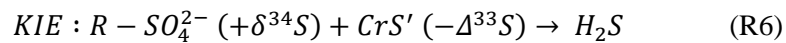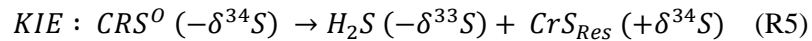
Reacted sulfur created during step one may then undergo magnetic isotope effects during

step 2 as well as kinetic isotope effects. As stated previously sulfur that experiences magnetic isotope

effects must also have been fractionated by the VEDE to have positive Δ^{33}S values. Therefore purple

MIE fractionation lines in figures 15a. and 15b. are only shown in pathways where VEDE have also fractioned sulfur. The sulfur species that has underwent the VEDE during step one but has not yet been fractionated by the magnetic isotope effect is labeled Cr^O.

The extent of fractionation this species has undergone due to kinetic isotope effects from CSO during step 2 is unknown but it assumed it may be substantial since the rupturing of the first S-O bound or reduction from S^{+6} to S^{4+} is the step that requires the highest activation energy during TSR (Ma et. al., 2009). The reacted sulfur that has been fractionated in the positive $\Delta^{33}S$ direction by the magnetic isotope effects is labeled as CrS' in figure 14. This fractionation is noticeable in the high temperature pathways and reduced or not present at all during low temperature reactions. Residual sulfur from the magnetic isotope effect during reaction R3 is labeled CrS*.

This is fractionated in the negative $\Delta^{33}S$ direction from CrS^O and CSO'. Residual sulfur from the kinetic isotope effect in step two that has already interacted with the organic matter will thus be fractionated in the positive $\delta^{34}S$ direction from reduction and maintain the same mass independent fractionation CSO acquired in reaction R2. This residual species that has interacted with organic matter but has underwent minimal reduction processes may be a sulfate ester which has been suggested as TSR intermediate based DFT molecular modeling calculations by Amrani et al., 2008, SO_3^{2-}, or SO_2 gas which would not be collected in our experiments.

Step 3:

$$KIE : CRS^O \ (-\delta^{34}S) \ \rightarrow H_2S \ (-\delta^{33}S) + \ CrS_{Res} \ (+\delta^{34}S) \quad (R5)$$

$$KIE : R - SO_4^{2-} \ (+\delta^{34}S) + CrS' \ (-\Delta^{33}S) \rightarrow \ H_2S \quad\quad (R6)$$

Step 3 would produce H_2S from all Cr-S species except CrS* through the kinetic isotope effect. At high temperatures H_2S would come from a combination of pathways originating from CrS^O, thus have the same $\Delta^{33}S$ signatures as CSO created Reaction R2, and CrS' which would be depleted in ^{33}S relative to CSO. At low temperatures where there are small amounts of CrS* produced H_2S will largely contain the same $\Delta^{33}S$ it acquired in step 1. This explains why experiments with high MIF-S signatures run at 200^OC and above have higher ranges in their $\Delta^{33}S$ values then low temperature experiments.

At high temperatures more CrS^O and CrS' would be converted to H_2S leaving the ^{33}S enriched CrS* species as the main chrome extracted sulfide product and likely less total CrS compared to H_2S than low temperature experiments as seen in the speciation results of 200^OC and 250^OC H_2SO_4 experiments from table 1. This would also create H_2S with less ^{34}S depletion than low temperature experiments due to kinetic fractionation. The opposing correlation with temperature between VEDE, which produces positive $\Delta^{33}S$, and $\delta^{34}S$ fractionation in reacted sulfur and normal mass dependent kinetic effects, which create ^{34}S depleted H_2S, is thus responsible for the positive $\Delta^{33}S_{H2S-H2S}/\Delta^{34}S_{H2S-H2S}$ fractionation observed with temperature in glycine and Na_2SO_4 experiments. The overlap in $\delta^{34}S$ ranges between 170^OC and 200^OC experiments may then be explained by a higher λ based on the temperature dependence of the VEDE. Lower $\delta^{34}S$ fractionation during reaction R1 and smaller kinetic effects during reduction in the high temperature experiment creates similar mass dependent fractionation observed in H_2S from the lower temperature experiment.

H_2S may also be produced from residual products of the kinetic and magnetic isotope effects in step two. As noted in reaction R3, reduction from sulfur fractionated from step one, CSO, will leave residual oxidized sulfur species such as SO_2, SO_3^{2-}, and sulfate esters with positive $\Delta^{33}S$ and positive $\delta^{34}S$ values. SO_2 gas would be carried out by helium in our experiments and not collected, aqueous SO_3^{2-} and organic sulfate compounds may be precipitated with $BaCl_2$ and collected as residual sulfate at the end of experiments. However R-SO_4^{2-} may undergo reduction and with the positive fractionation it incurred in step 2 the H_2S produced in this processes contain less depleted ^{34}S values than those resulting from the

direct reduction of CSO. Sulfate esters will also be reduced through reactions with other reduced sulfur species such as thiols. This process will form thiosulfate, which would quickly be reduced to H_2S (Amrani et al., 2008) which would thus bear an isotopic composition from the mixture of R-SO_4^{2-} bearing positive $\delta^{34}S$ fractionation from R2 and residual fractionation from R3 and the reduced sulfur compound bearing negative fractionations. Based on the relative fractionation of these two contributions the quick reduction of R-SO_4^{2-} may produce H_2S that is ^{34}S enriched compared to the products of VEDE (CSO). If any spin selective processes occurred before the thiol compound was produced then this species may represent residuals of magnetic isotope effect in reaction R3, CrS*, with ^{33}S depleted fractionations relative to the products of the VEDE. CrS* that does not get reduced to H_2S would then incur some positive $\delta^{34}S$ fractionation from the residual product of reaction R5. Therefor products of this reaction, represented in reaction R6 and shown schematically in figure 14d. may be ^{34}S enriched and ^{33}S depleted relative to H_2S produced from other pathways. This would account for negative $\Delta^{33}S_{H2S-H2S}/\Delta^{34}S_{H2S-H2S}$ fractionation trends observed M-SSA-200 experiments where very large $\delta^{34}S$ values are observed.

As observed in figure 15 the schematic described above is able to create the complete range of isotope values and trends observed in the products of TSR experiments. Residuals from VEDE and the kinetic isotope effects in steps 1 and 2 (dotted lines in figure 14A) contribute to the isotopic composition of sulfate collected at the end of experiments. $\delta^{34}S$ fractionation resulting in the ^{34}S enrichment of sulfate is due to kinetic processes occurring largely in R1. The observed negative $\Delta^{33}S$ values are due to the contribution of the residual product from the VIDE. However the mass dependent contribution of the VEDE opposes the kinetic effects (although trends in $\delta^{34}S$ values of sulfate in high temperature experiments may be aided by larger λ at these conditions). This would explain why the relative $\delta^{34}S$ fractionation between residual sulfate does show typical Rayleigh behaviors (i.e. why sulfate is not as fractionated as bulk H_2S at $[SO_4^{2-}/H_2S] > 1$). Contribution of residual oxidized sulfur in step two, i.e. reacted sulfur from the VEDE in step one that does not get reduced or leave the experiment, back to the

sulfate pool would dilute the mass independent effects on sulfate incurred in step one. This then explains

the small fractionations of sulfate relative to reduced sulfur collected during TSR.
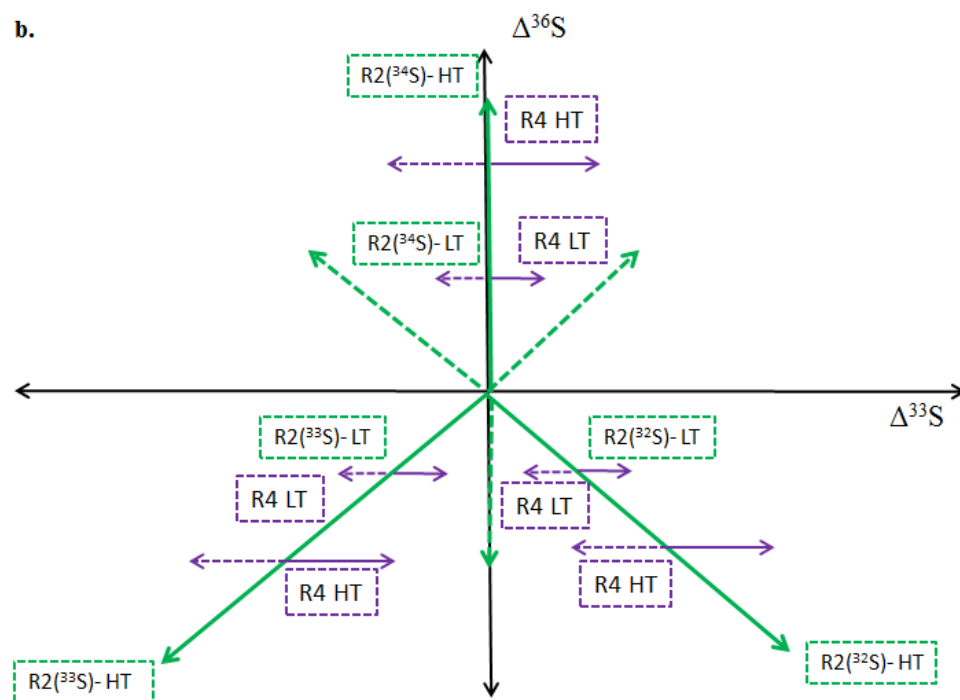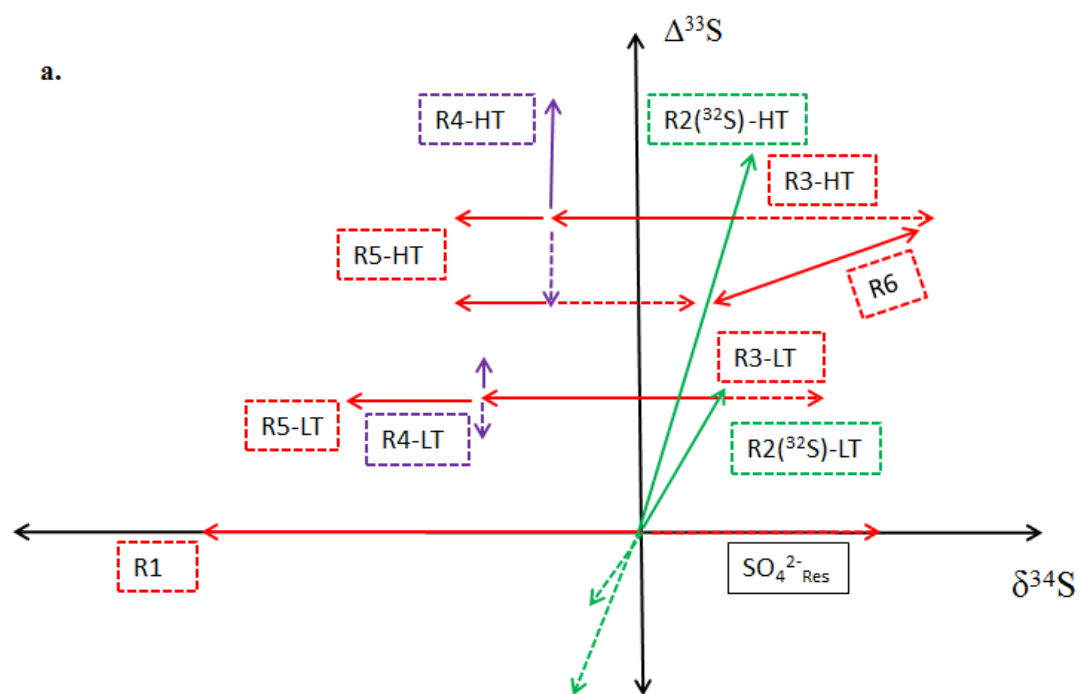
Figure 15: Synthesis Schematics for Isotope Fractionation During TSR

Pathway for isotope fractionations of various sulfur species during TSR in the $\Delta^{33}S$ vs. $\delta^{34}S$ (a.) and $\Delta^{36}S$ vs. $\Delta^{33}S$ Cartesian Plots. Solid arrows show fractionations of products of the labeled reactions while dotted lines show direction of residual products. Reaction labeled HT show extent of fractionation for high temperature reactions and are shown with shorter solid and longer dotted red arrows (KIE effects) and longer green (VEDE effects) and purple (MIE) lines. Reactions labeled LT show extent of fractionation for low temperature reactions and shown with longer solid and shorter dotted red arrows and shorter green and purple arrows. The end of red solid arrows show the isotope composition of H_2S due to the various reaction pathways in a. while the end of dotted purple arrows show the composition of H_2S in b.

6   Conclusions and implications for the Archean

Figure 16 summarizes Archean isotope data in the Δ^{33}S vs δ^{34}S and Δ^{36}S vs. Δ^{33}S Cartesian. From both these figures many fractionation trends can be observed in sulfides containing MIF-S Δ^{33}S and Δ^{36}S values. Sulfates characteristically contain positive δ^{34}S between 3 and 8‰ and negative Δ^{33}S values between 0 and -1‰. Sulfates with positive Δ^{33}S values are also ^{34}S enriched but contain fractionation up to 15‰. Sulfides are observed containing both ^{34}S enrichments and depletions from V-CDT as well as the presumed value for Archean ocean sulfate (Claypool 1980, Canfield and Raiswell 1999). They bear positive and negative Δ^{33}S values with respect to sulfate. However larger δ^{34}S ranges are observed in sulfides that contain little mass independent fractionation from the terrestrial fractionation line or Archean sulfates. Researchers have noted that many late Archean sulfides with large MIF-S signatures fall on a Δ^{33}S/^{34}S and Δ^{36}S/Δ^{33}S trend lines of +1 and -.8 respectively (Ono et al., 2003). These samples come largely from sulfide and organic rich black shales of the Hamersley basin in Western Australia and Transvaal basin of South Africa and make up what is known as the Hamersley trend. Sulfides containing δ^{34}S values lighter than this trend contain Δ^{33}S$_{H2S-H2S}$/Δ^{34}S$_{H2S-H2S}$ fractionation of roughly the same Δ^{33}S/^{34}S slope as the Hamersley trend while the Δ^{33}S$_{H2S-H2S}$/Δ^{34}S$_{H2S-H2S}$ fractionation of samples heavier than the Hamersley trend in roughly the opposite direction. There are also many Archean sulfides containing Δ^{36}S/Δ^{33}S ratios that fall above and below the Hamersley trend however the deviation of sulfate minerals from this slope is not as pronounced.

These features of the Archean sulfur isotope record may be explained using the previously described schematic of the three active fractionation mechanisms occurring during TSR. This can be done because 1. The Δ^{33}S/^{34}S and Δ^{36}S/Δ^{33}S Hamersley trends are in the same direction as those created by VEDE-32 in reaction R2. Since VEDE is active in the first step of TSR, if kinetic effects of the second and third steps, i.e. reduction, are small than we would only observe isotopic trends in MIF-S containing samples that follow the fractionation trend of R2. Based on evidence that suggest the Hamersley and Gringiland where rift basins that experienced regular cycles of stratified brackish, euxenic deep water

overlade by oxygen rich surface water (Ohmoto et al., 2006b) and the high sulfide content of the shales it is suggested that TSR occurred in high productivity closed system conditions by the circulation of sulfate through organic rich sediment. If terrestrial fluxes of sulfur, i.e. mass dependently fractionated sulfate, were periodically shut off to the deep water during periods of persistent brine conditions then multiple cycles of TSR may occur through continual hydrothermal circulation and oxidation of sulfide at the brine-seawater interface. This would cause MIF-S signatures to accumulate through reaction R2 with little kinetic fractionation.

The range of δ^{34}S values increases for samples with smaller MIF-S values. This occurs through the reduction of mass dependent fractionation for sulfides with both negative and positive δ^{34}S values relative to the Hamersley trend creating the positive and negative Δ^{33}S$_{H2S-H2S}$/Δ^{34}S$_{H2S-H2S}$ trends marked in figure 16a. These are similar to the two trends observed in our TSR results which have been explained through the kinetic effects on fractionations of products from reactions R5 and R3 and the residuals of R3 and R5 creating sulfide through reaction R6. As previously described in the synthesis the residuals of R3 may also create sulfate enriched in ^{34}S relative to VEDE, this explains why the heaviest sulfate in the Archean have positive Δ^{33}S values. The maximum δ^{34}S ranges observed in the Archean then can be attributed through low temperature abiotic and bacterial sulfate reduction which create little mass independent fractionation and higher mass dependent fractionation (Machel, Krouse, and Sassen 1994).

The Δ^{36}S/Δ^{33}S trend observed in samples with large MIF-S signatures may also be explained by the prevalence of VEDE of the ^{32}S isotope during R2 at the expense of kinetic fractionations. Fractionations away from this trend especially in the lower right quadrant of the Δ^{36}S vs. Δ^{33}S Cartesian may be caused by the MIE during reaction R4. Samples with large MIF-S samples fractionated in 1 and 2 (similar to those from M-SSA-200 experiments) may have been fractionated in reaction R2 by the VEIDE of the ^{34}S isotope and experience subsequent fractionation from the MIE. Consistent Δ^{36}S/Δ^{33}S trends observed in other samples (Kurweil et al., 2013) may be created through fractionations by TSR occurring at conditions different then those responsible for the Hamersley trend or contributions of mass dependent

kinetic effects during TSR which create steeper $\Delta^{36}S/\Delta^{33}S$ ratios (Oduro et al., 2011, Farquhar et al., 2007, Ono et al., 2006).

7. Broad Impact

Our experiments therefore support the hypothesis that many MIF-S signatures observed in Archean are due to the various fractionations observed in TSR experiments. Therefore the Archean oceans were rich in sulfate likely derived non MIF-S creating sources. This infers that specific fractionations observed in samples are a function of depositional environment and not necessarily atmospheric chemistry. These deposition factors include: 1. maturation history, as confirmed by the effects of temperature on fractionation during TSR, 2. hydrothermal circulation and alteration though changes in oxygen fugacity and pH which effect sulfur speciation and redox state, and 3. the content of the original deposition. Our results may therefor be used to distinguish sedimentary basins through time for these factors based on the presence of MIF-S. They also provide experimental evidence for a direct link between the presence and magnitude MIF-S signatures and the fate of organic matter which may be used to aid in the interpretation of the Archean carbon isotope record. The high preservation rate of Archean sediments containing large MIF-S signatures supports the hypothesis that plate tectonics was slower and the lithosphere was thicker and more hydrous during the Archean (Korenaga 2008). These conditions would allow for the creation of long lived hydrothermal rift basins where TSR would likely take place. The failure of these rift systems to create new oceanic crust would therefore preferentially preserve MIF-S containing sediments in the cratonic mass.

a.

b.
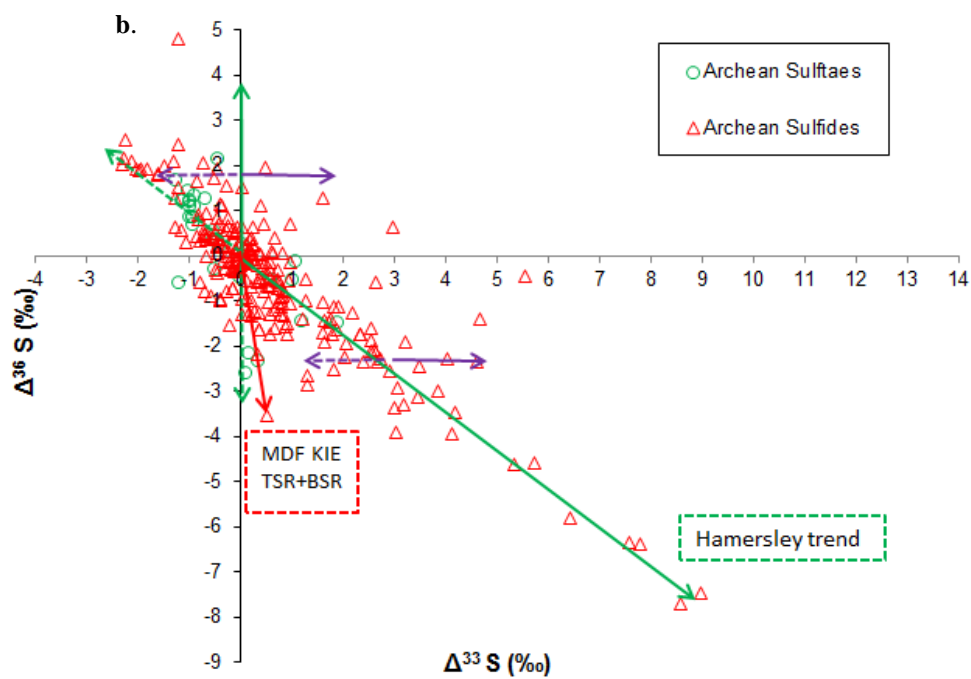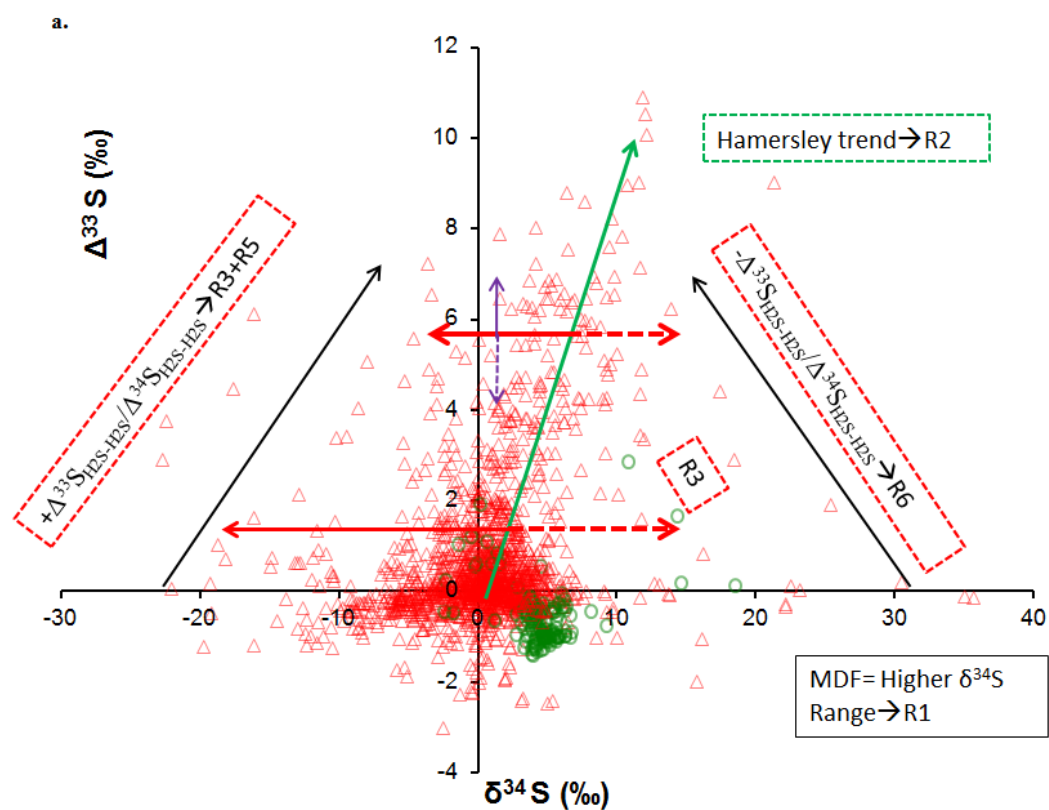
Figure 16: Archean Multiple Sulfur Isotope Data Compilation

$\Delta^{33}S$ vs. $\delta^{34}S$ (a.) and $\Delta^{36}S$ vs. $\Delta^{33}S$ (b.) Cartesian Plots modified from Ohmoto et. al., 2014 with various TSR fractionation trends labeled . Green arrows show trends of VEDE which are similar to late Archean Hamersley trends. Black arrows in a. show the prominent $\Delta^{33}S_{H2S-H2S}/\Delta^{34}S_{H2S-H2S}$ of Archean data with the labeled kinetic reactions that produce the same trends (pathways labeled with red arrows). The large $\delta^{34}S$ range is noted along x-axis and attributed to mass dependent fractionation of Archean sulfur. Red arrow in b. shows the proposed mass dependent kinetic fractionation line for biological and thermochemical sulfate reduction that is similar in slope to many Archean samples. Puple arrows display how the MIE may cause variation in $\Delta^{36}S/\Delta^{33}S$ ratios.

References

Amrani, A., Zhang, T., Ma, Q., Ellis, G.S., Tang, Y., 2008, The role of labile sulfur compounds in thermochemical sulfate reduction: Geochimica et Cosmochimica Acta, v. 72, p. 2960-2972

Anisimov, L.A., 1978, Conditions of abiotic reducitons of sulfate in oil-an-gas bearing basins, Geokhimiya, v. 11, p. 1692-1702

Baroni, M., Savarino, J., Cole-Dai, J., Rai, V.K., and Thiemens, M.H., 2008, Anomalous sulfur isotope compositions of volcanic sulfate over the last millennium in Antarctica ice cores: Journal of Geophysical Research v. 113, p. D20112

Bontognali, T.R.R., Sessions, A.L., Allwood, A.C., Fischer, W.W., Grotzinger, J.P., Summons, R.E., and Eller, J.M., 2012, Sulfur isotopes of organic matter preserved in 3.45-billion-year- old stromatolites reveal microbial metabolism: Proceedings of the National Academy of Sciences of the United States of America, v. 109, p. 15,146–15,151

Canfield D. E., Raiswell R., Westrich J. T., Reaves C. M., and Berner R. A., 1986, The use of chromium reduction in the analysis of reduced inorganic sulfur in sediments and Shales: Chemical Geology, v. 54, p.149–155

Canfield, D.E., and Raiswell, R., 1999, The evolution of the sulfur cycle: American Journal of Science, v. 299, p. 697–723

Claypool, G., Holser, W., Kaplan, I., Sakai, H., and Zak, I., 1980, The age curves of sulfur and oxygen isotopes in marine sulfate and their mutual interpretation: Chemical Geology, v. 28, p. 199–260

Czaja, A.D., Johnson, C.M., Roden, E.E., Beard, B.L., Voegelin, A.R., Nagler, T.F., Buekes, N.J., Wille, M., 2012, Evidence for free oxygen in the Neoarchean ocean based on coupled iron-molybdenum isotope fractionation: Geochimica et Cosmochimica Acta, v. 86, p. 118-137

Farquhar, J., Bao, H., and Thiemens, M., 2000, Atmospheric influence of Earth's earliest sulfur cycle: Science, v. 289, p. 756–758,

Farquhar, J., Johnston, D.T., and Wing, B.A., 2007, *Implications of conservation of mass effects on mass-dependent isotope fractionations: Influence of network structure on sulfur isotope phase space of dissimilatory sulfate reduction: Geochimica et Cosmochimica Acta, v. 71,   p. 5862–5875*

Frei, R., Gaucher, C., Poulton, S.W., Canfield, D.E., 2009, *Fluctuations in Precambrian atmospheric oxygen recorded by chromium isotopes: Nature, v. 461, p. 250-253*

Goldhaber, M.B., Orr, W.L., 1995, *Kinetic controls on thermochemical sulfate reduction as a source of sedimentary H_2S: Geochemical Transformations of Sedimentary Sulfur, v. 612*

Goldstein, T.P., Aizenshtat, Z., 1994, *Thermochemical sulfate reduction-a review: J. Thermal. Anal., v. 42, p. 241-290*

Kendall, B., Reinhard, C.T., Lyons, T.W., Kaufman, A.J., Poulton, S.W., Anbar, A.D., 2010, *Pervasive oxygenation along late Archean ocean margins: Nature Geoscience, v. 3, p. 647-652*

Kerrich, R., Said, N., 2011, *Extreme positive Ce-anomalies in 3.0 Ga submarine volcanic sequence, Murchison Province: Oxygenated marine bottom waters: Chemical Geology, v. 280, p. 232-241*

Korenaga, J., 2008, *Plate tectonics, flood basalts and the evolutions of Earth's oceans: Terra Nova, v. 20, p. 419-439*

Kurzweil, F., Claire, M., Thomazo, C., Peters, M., Hannington, M., Strauss, H., 2013, *Atmospheric sulfur rearrangement 2.7 billion years ago: Evidence for oxygenic photosynthesis: Earth and Planetary Science Letters, v. 366, p. 17-26*

Lasaga, A.C., Otake, T., Watanabe, Y., and Ohmoto, H., 2008, *Anomalous fractionation of sulfur isotopes during heterogeneous reactions: Earth and Planetary Science Letters, v. 268, p. 225–238*

Ma, Q., Ellis, G.S., Amrani, A., Zhang, T., Tang, Y., 2009, *Theoretical study on the reactivity of sulfate species with Hydrocarbons: Geochimica et Cosmochimica Acta*

Machel, H.G., Krouse, H.R., Sassesn, R., 1995, *Products and distinguishing criteria of bacterial and thermochemical sulfate reduction: Applied Geochemistry, v. 10, p. 373-389*

Masterson, A.L., Farquhar, J., and Wing, B.A., 2011, *Sulfur mass-independent fractionation patterns in the broadband UV photolysis of sulfur dioxide: Pressure and third body effects: Earth and Planetary Science Letters, v. 306, p. 253–260*

Oduro, H., Harms, B., Sintim, H.O., Kaufman, A.J., Cody, G., and Farquhar, J., 2011, *Evidence of magnetic isotope effects during thermochemical sulfate reduction: Proceedings of the National Academy of Sciences of the United States of America, v. 108, p. 17,635–17,638*

Ohmoto, H., Watanabe, Y., Ikemi, H., Poulson, S.R., and Taylor, B.E., 2006a, Sulphur isotope evidence for an oxic Archaean atmosphere: Nature, v. 442, p. 908–911

Ohmoto, H., Watanabe, Y., Yamaguchi, K.E., Naraoka, H., Haruna, M., Kakegawa, T., Hayashi, K., and Kato, Y., 2006b, Chemical and biological evolution of early Earth: Constraints from banded iron formations, in Kesler, S.E., and Ohmoto, H., eds., Evolution of Early Earth's Atmosphere, Hydrosphere, and Biosphere: Constraints from Ore Deposits: Geological Society of America Memoir 198, p. 291–331

Ohmoto, H., Watanabe, Y., Lasaga, A.C., Naroaka, H., Johnson, I., Brainard, J., Chorney, A., 2014, Oxygen, iron, and sulfur geochemical cycles on early Earth: Paradigms and contradictions: GSA Special Papers, v. 504, p. 55-95

Ono, S., Eigenbrode, J., Pavlov, A.A., Kharecha, P., Rumble, D., Kasting, J.F., and Freeman, K.H., 2003, New insights into Archean sulfur cycle from mass-independent sulfur isotope records from the Hamersley Basin, Australia: Earth and Planetary Science Letters, v. 213, p. 15–30

Ono, S., Wing, B., Johnston, D., Farquhar, J., and Rumble, D., 2006, Mass-dependent fractionation of quadruple stable sulfur isotope systems as a new tracer of sulfur biogeochemical cycles: Geochimica et Cosmochimica Acta, v. 70, p. 2238–2252

Ono, S., Whitehill, A.R., Lyons, J.R., 2013, Contribution of isotopologue self-shielding to sulfur mass-independent fractionation during sulfur dioxide photolysis: Journal of Geophysical Research: Atmospheres, v. 118, p. 2444-2454

Otake, T., Lasaga, A., Ohmoto, H., 2008, Ab initio calculations for equilibrium fractionations in multiple sulfur isotope systems: Chemical Geology, v. 249, p. 357-376.

Pavlov A. A. and Kasting J. F., 2002, Mass-independent fractionation of sulfur isotopes in Archean sediments: Strong evidence for an anoxic Archean atmosphere. Astrobiology, 2, 27–41

Thode, H., Monster, J., and Dunford H. B., 1961 Sulphur isotope geochemistry: Geochimica Cosmochimica Acta, v. 25, p. 159–174

Watanabe, Y., Farquhar, J., and Ohmoto, H., 2009, Anomalous fractionations of sulfur isotopes during thermochemical sulfate reduction: Science, v. 324, p. 370–373

Whitehill, A.R., and Ono, S., 2012, Excitation band dependence of sulfur isotope mass-independent fractionation during photochemistry of sulfur dioxide using broadband light sources: Geochimica et Cosmochimica Acta, v. 94, p. 238–253

Young, S.A., Loukola-Ruskeeniemi, K., Pratt, L.M., 2013, Reactions of hydrothermal solutions with organic matter in Paleoproterozoic black shales at Talvivaara, Finland: Evidence from multiple sulfur isotopes: Earth and Planetary Science Letters, v. 367, p. 1-14

Appendix A

Supplemental Methods
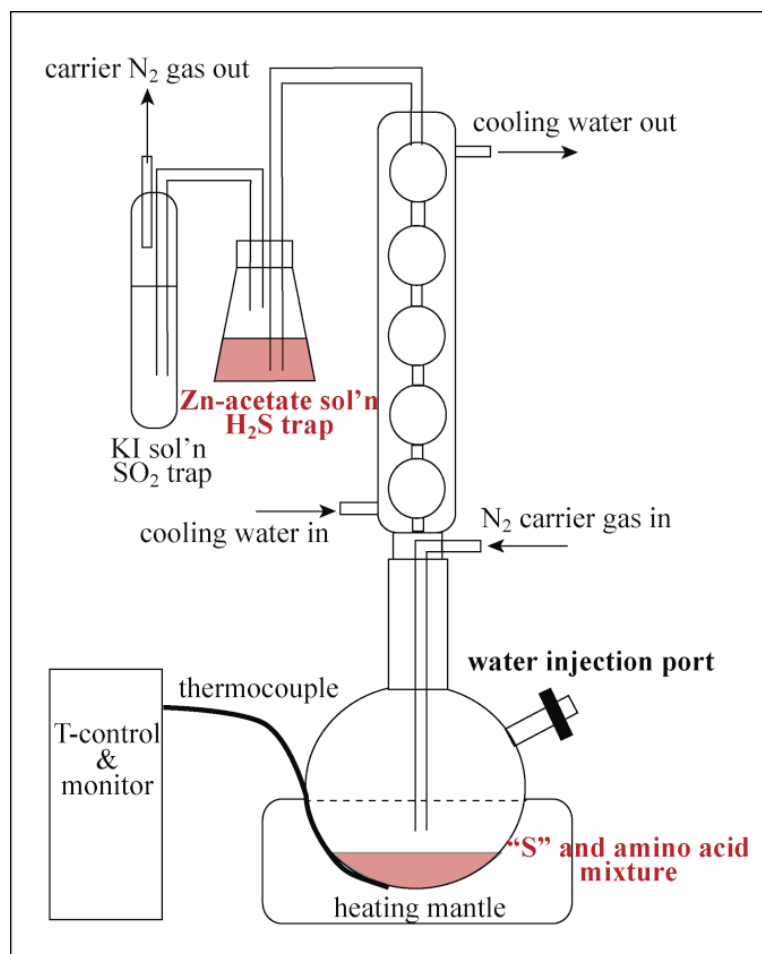
Supplemental Figure 1: Experimental Apparatus
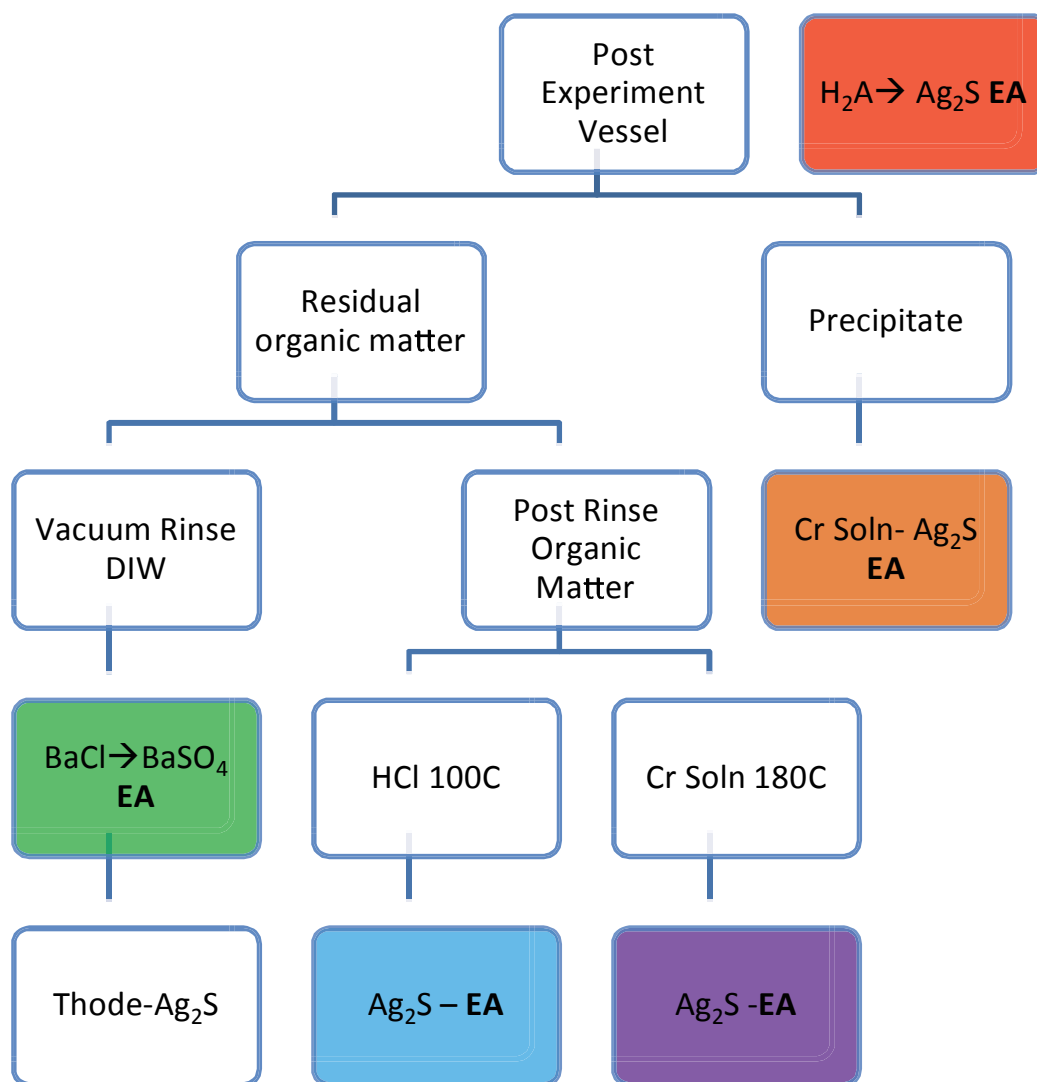
Supplemental Figure 2: Sample Collection Sequence

Appendix B

Isotope Data

Experiment ID	Sample	Starting S (mmol)	Starting Carbon (mmol)	Time of Collection (hr)	Sample amount (mmol S)	$\delta^{34}S_{PSU}$	$\Delta^{33}S_{PSU}$	$\delta^{34}S_{UMD}$	$\Delta^{33}S_{UMD}$	$\Delta^{36}S_{UMD}$
M-SSA-200-1		7.429	82.935							
	H_2S-1			1	0.005	-9.53	2.21			0.457
	H_2S-2			3	0.002	NM	NM			
	H_2S_{Total}			C	0.007	NM	NM			
	$SO_4^{2-}{}_{Residual}$			3	NM	4.28	-0.07			
M-SSA-200-2		7.404	83.018							
	H_2S-1			1	0.006	-10.58	2.30			
	H_2S-2			3	0.004	-5.82	2.08			
	H_2S_{Total}			C	0.010	-8.64	2.21			
	$SO_4^{2-}{}_{Residual}$			3	NM	-0.27	0.00			
M-SSA-200-3		7.063	111.206							
	H_2S-1			5	0.007	-7.33	1.54			
	H_2S-2			10	0.004	-7.69	2.20			
	H_2S_{Total}			C	0.011	-7.46	1.78			
	$SO_4^{2-}{}_{Residual}$			10	5.708	3.48	-0.09			
	MissingS			C	1.344	-14.72	0.37			
M-SSA-200-4		7.125	110.903							
	H_2S-1			5	0.012	15.50	0.48			
	H_2S-2			10	0.017	2.59	1.20			0.379
	H_2S-3			24	0.016	0.89	1.87			1.39
	H_2S-4			29	0.005	NM	NM			
	H_2S-5			48	0.007	5.06	0.93			
	H_2S_{Total}			C	0.057	4.91	1.10			
	$SO_4^{2-}{}_{Residual}$			48	7.060	0.37	0.00			
	MissingS			C	0.008	-362.39	-7.86			

Experiment ID	Sample	Starting S (mmol)	Starting Carbon (mmol)	Time of Collection (hr)	Sample amount (mmol S)	$\delta^{34}S_{PSU}$	$\Delta^{33}S_{PSU}$	$\delta^{34}S_{UMD}$	$\Delta^{33}S_{UMD}$	$\Delta^{36}S_{UMD}$
M-SSA-200-5		14.808	83.046							
	H_2S-1			NM	NM	-7.33	1.54			
	H_2S-2			25	NM	-5.01	1.03			1.39
G-HSA-300-1		2.133	40.107							
	H_2S-1			2.5	0.841	-2.35	-0.02			
	H_2S-2			5.5	0.032	-10.28	0.07			
	H_2S_{Total}			C	0.873	-2.64	-0.02			
	MissingS			C	1.260	1.83	0.01			
G-HSA-200-1		2.261	40.107							
	H_2S-1			0.75	0.221	-6.5	0.1			
	H_2S-2			1	0.137	-3.01	0.06			
	H_2S-3			51.75	0.017	-9.75	0.08			
	H_2S-4			79.75	0.01	-3.41	0.09			
	H_2S-5			107.75	0.01	-4.98	0.06			
	H_2S_{Total}			C	0.395	-5.313	0.084			
	CrS			107.5	0.162	0.26	0.07			
	ReducedS$_{Total}$			C	0.557	-3.69	0.08			
	MissingS			C	1.705	1.20688	-0.02613			
G-ASA-200-1		2.206	40.267							
	CrS			96	0.165	-15.47	0.2			
	$SO_4^{2-}{}_{Residual}$			96	0.068	6.61	-0.01			
	MissingS			C	1.97298	1.06597	-0.01638			
G-ASA-200-2		2.181	40.166							
	CrS			49	0.009	NM	NM			
	$SO_4^{2-}{}_{Residual}$			49	0.851	1.71	0.01			

Experiment ID	Sample	Starting S (mmol)	Starting Carbon (mmol)	Time of Collection (hr)	Sample amount (mmol S)	$\delta^{34}S_{PSU}$	$\Delta^{33}S_{PSU}$	$\delta^{34}S_{UMD}$	$\Delta^{33}S_{UMD}$	$\Delta^{36}S_{UMD}$
G-ASA-200-3		2.046	40.097							
	CrS			49	0.248	-8.73	0.14			
	$SO_4^{2-}{}_{Residual}$			49	0.22	5.65	-0.02			
	MissingS			C	1.577712	0.58595	-0.01924			
G-ASA-250-1		2.026	40.143							
	H_2S-1				0.019	-8.95	0.08			
	S^0			C	0.089	-2.13	0.12			
	CrS				0.258	-5.51	0.1			
	ReducedS$_{Total}$			C	0.366	-5.16	0.1			
	$SO_4^{2-}{}_{Residual}$				0.035	7.85	-0.15			
	MissingS			C	1.294006	2.246	-0.04473			
M-ASA-250-1		2.339	45.833							
	H_2S-1			0.25	0.086543	-9.9	0.19			
	H_2S-2			0.5	0.15952	NM	NM			
	H_2S-3			0.75	0.157157	-6.47	0.21			
	H_2S-4			1.25	0.166537	NM	NM	-3.9737	0.16	-0.35
	H_2S-5			2.58	0.054662	1.12	0.18			
	H_2S-6			4.75	0.034874	NM	NM			
	H_2S-7			11.5	0.015648	2.34	-0.22			
	H_2S-8			57.5	0.014034	1.22	-0.22			
	H_2S_{Total}			C	0.688976	-5.352	0.1			
	S^0			C	0.03836	-1.04	0.16	-1.799	0.11	-0.17
	HClS			57.5	0.069936	5.63	-0.13			
	CrS			57.5	0.047716	5.3	-0.08	5.56033	-0.1	-0.26
	ReducedS$_{Total}$			C	0.846	-3.07	0.06			
	$SO_4^{2-}{}_{Residual}$			57.5	0.203961	3.3	-0.09			
	MissingS			C	1.289959	1.86627	-0.03393			

Experiment ID	Sample	Starting S (mmol)	Starting Carbon (mmol)	Time of Collection (hr)	Sample amount (mmol S)	$\delta^{34}S_{PSU}$	$\Delta^{33}S_{PSU}$	$\delta^{34}S_{UMD}$	$\Delta^{33}S_{UMD}$	$\Delta^{36}S_{UMD}$
M-ASA-250-2		2.208	45.824							
	H_2S-1			0.25	0.185	-7.94	0.17			
	H_2S-2			0.5	0.21	NM	NM	-0.381	0.11	-0.65
	H_2S-3			0.75	0.166	NM	NM			
	H_2S-4			1.25	0.124	-0.52	-0.04			
	H_2S-5			2.58	0.052	NM	NM			
	H_2S-6			4.75	0.014	1.51	-0.21			
	H_2S-7			11.5	0.007	NM	NM			
	H_2S-8			57.5	0.013	1.58	-0.17			
	H_2S_{Total}			C	0.771	-4.44	0.06			
	S^0			C	0.065	-0.57	0.13			
	HClS			57.5	0.016	6.64	-0.16			
	CrS			57.5	0.041	5.59	-0.09			
	ReducedS$_{Total}$			C	0.893	-2.88	0.08			
	$SO_4^{2-}{}_{Residual}$			57.5	0.192	3.85	-0.09			
	MissingS			C	1.098701	2.05844	-0.02569			
M-ASA-200-1		2.053	45.806							
	H_2S-1			11.5	0.028	-12.14	0.1			
	H_2S-2			23.5	0.039	-13.14	0.08			
	H_2S_{Total}			C	0.067	-12.72	0.09			
	S^0			C	0.018272	-6.15	0.11			
	HClS			23.5	0.018888	-4.85	0.1			
	CrS			23.5	0.179432	-4.44	0.14			
	ReducedS$_{Total}$			C	0.283	-6.53	0.12			
	$SO_4^{2-}{}_{Residual}$			23.5	0.622675	6.64	-0.06			
	MissingS			C	1.146806	-1.98971	0.00202			

Supplemental table 1: Full Experimental summary